Øystein Smith

# Analysis of design parameters in a musical dual resonant solid state tesla coil

Master thesis

Trondheim, June 2017

Norwegian University of Science and Technology
Faculty of Information Technology and Electrical Engineering
Department of Electronic Systems

NTNU
Innovation and Creativity

**NTNU**

Norwegian University of Science and Technology

Master thesis
for the degree of Master of Technology

Faculty of Information Technology and Electrical Engineering
Department of Electronic Systems



ISBN (printed version)
ISBN (electronic version)
ISSN 1503-8181

Master theses at NTNU,

Printed by NTNU-trykk

## Abstract

Universities, science centers and other institutions has the need for equipment that demonstrates physical phenomena in interesting and audience friendly ways. An example of this is a Double Resonant Solid State Tesla Coil (DRSSTC). There is no big commercial or academic community for tesla coils, but tesla coils are mostly designed and used as a hobby. There are a few people sharing their designs on the internet that most of the tesla coil designs are based on. Few or none of these substantiate design choices or assumptions with physics and math. This thesis will attempt to substantiate the design choices done in the driver for a musical dual resonant solid state tesla coil.

This thesis discusses an implementation of a DRSSTC, substantiates the functionality of sub circuits and components with mathematics. Then discusses the mathematical description of the resonant transformer, varying component sizes, plotting and simulating the transfer functions. Then presents some measurements done on a physical implemented DRSSTC.

The component values or parameters that need to be adapted to the resonant frequency are; the delay in the latch reset network in the interrupter, the phase lead time in the interrupter, and the corner frequency of the noise filter in the limiter. The component values or parameters that need to be adapted to the current flowing in the primary resonant circuit are; the impedance of the feedback load in the interrupter and in the limiter, and the number of turns on the current feedback transformers.

In the resonant circuit we have proven that the ohmic resistances in both the primary and secondary circuit should be as small as possible to give a high as possible amplitude on the output, the conductance of the streamer does not seem to affect the resonant frequency (detuning) or the amplitude on the output, but does affect the current in the primary resonant circuit. And will affect the feedback signals. The coupling coefficient only affects the amplitude on the output, as long as no arcing happens between the primary and secondary coils. According to the transfer functions varying the capacitors or inductors does not give the same results as expected from the common assumptions in the hobby community. Here no other conclusions can be drawn other that this may be a topic for further research.

## Sammendrag

Universiteter, vitenskapssentre og andre institusjoner har behov for utstyr som demonstrerer fysiske fenomener på interessante og publikumsvennlige måter. Et eksempel på dette er en Double Resonant Solid State Tesla Coil (DRSSTC). Det er ikke noe stort kommersielt eller faglig miljø for tesla-spoler, men tesla-spoler er for det meste utformet og brukt som en hobby. Det er noen få personer som deler design på internett som de fleste tesla-spoledesign er basert på. Få eller ingen av disse underbygger designvalg eller antagelser med fysikk og matte. Denne oppgaven vil forsøke å underbygge designvalgene som er gjort i driveren til en musikalsk Dual Resonant Solid State Tesla Coil.

Denne oppgaven diskuterer en implementering av en DRSSTC, underbygger funksjonaliteten til underkretser og komponenter med matematikk. Deretter diskuteres den matematiske beskrivelsen av resonanttransformatoren, komponentstørrelser varieres, overføringsfunksjonene plottes og simuleres. Deretter presenteres noen målinger gjort på en fysisk implementert DRSSTC.

Komponentverdiene eller parametrene som må tilpasses resonansfrekvensen er; forsinkelsen i sperreinnstillingsnettverket i avbryteren, faseovergangstiden i avbryteren og hjørnefrekvensen av støyfilteret i begrenseren. Komponentverdiene eller parametrene som må tilpasses til strømmen i den primære resonanskretsen er; impedansen til tilbakekoblingsbelastningen i avbryteren og i begrenseren, og antall viklinger på tilbakekoblingstransformatorene.

I resonanskretsen har vi vist at de ohmske motstandene i både primær- og sekundærkretsen bør være så små som mulig for å gi en høy som mulig amplitude på utgangen, konduktansen til gnisten ser ikke ut til å påvirke resonansfrekvensen (detuning) eller amplitude på utgangen, men påvirker strømmen i den primære resonanskretsen. Og vil påvirke tilbakekoblingssignalene. Koblingskoeffisienten påvirker bare amplituden på utgangen, så lenge det ikke oppstår lysbue mellom primær- og sekundærspolene. I henhold til overføringsfunksjonene gir ikke variasjon av kondensatorene eller spolene de samme resultatene som forventet fra de vanligste antagelsene i hobbymiljøet. Her kan det ikke trekkes andre konklusjoner enn at dette kan være et tema for videre forskning.

## Preface

Omega Verksted has a long tradition with providing Tesla Coil shows for the line union 'Omega' and for other student societies at NTNU. The current implementation is based on some inadequate documentation from the 2009 implementation. The 2009 implementation was in use up to 2014 and was notorious for blowing output transistors. As well as for being put together with hot glue. In 2014 an effort was begun to improve the reliability and portability of the tesla coil. A new implementation was created with the design split into modules to ease the further development. The connectors and the casing for the driver was replaced and a back plane architecture was selected improving portability and reliability greatly. And a project report was written on the back plane architecture [20]. The coil rig was also replaced as it had the tendency to catch fire. The mode of operation for this implementation of a DRSSTC or general DRSSTC implementations are still not understood fully by all members of the project. This thesis aims do provide adequate documentation on the current DRSSTC implementation at Omega Verksted. And to serve as an educational document to give project members the knowledge to change or improve on the implementation.

Thanks should be made to Omega Verksted who has financed the parts used for this project, Tim Cato Nedland at the department of acoustics who did the acoustic measurements, the department of electrical power engineering who provided a safe location to do measurements, and HSE coordinator Sverre Vegard Pettersen who helped to make it feasible to do safe measurements. Lastly thanks should be made to my supervisor Lars Lundheim who have provided invaluable support and guidance through the work on this thesis.

# Contents

# List of Tables

# List of Figures

# Chapter 1

# Introduction

Universities, science centers and other institutions has the need for equipment that demonstrates physical phenomena in interesting and audience friendly ways. An example of this is a Double Resonant Solid State Tesla Coil (DRSSTC). This is a contraption that by the use of high voltage generates a sequence of electrical discharges. When these discharges happen in air a sound wave is generated. By modulating the frequencies of these discharges one can generate sound with different tones. A DRSSTC can in this way be made into a musical instrument. There is no big commercial or academic community for tesla coils, but tesla coils are mostly designed and used as a hobby. There are a few people sharing their designs on the internet that most of the tesla coil designs are based on. Few or none of these substantiate design choices or assumptions with physics and math. This thesis will attempt to substantiate the design choices done in the driver for a musical dual resonant solid state tesla coil.

Figure 1.1 shows a DRSSTC in use with an electric discharge from the top to a grounded copper object.

## 1.1 Tesla Coil

The Tesla Coil is a form of resonant transformer invented by Nikolai Tesla and used for experiments with artificial illumination [13]. A resonant transformer consists of two inductively coupled coils, each loaded with a capacitance such that they get the same resonance frequencies. The resonant transformer has since gotten a lot of applications, among others; RFID [2], NFC [16], and Wireless charging [8]. The resonant transformer in the form of the Tesla Coil has also become a popular entertainment device.

**Figure 1.1:** A tesla coil in use
Photo: Sindre Vaskinn Hunn

## 1.2 Earlier work

Some of the people who have done work on DRSSTC in the hobbby community are; Steve Ward [17], Jimmy Hynes [9], Terry Fritz [5], Steve Conner [4], Dan McCauley [11], and the tesla coil mailing list [1]. Among these there are few disagreements on how a tesla coil should be designed, there are few variations on the resonant circuit, but slightly more variation on the low voltage controlling side. Some use a preset oscillator to drive the resonant circuit, while others use feedback from either the primary or secondary resonant circuits.

There has been developed an drsstc tesla coil driver by Steve Ward witch other people have designed variations on [7]. Simulation software for the resonant circuitry of tesla coils called Scantesla have been written [12]. Guidelines for the design of the resonant circuits can be found at most of the above mentioned sites.

A modular back plane based tesla coil driver implementation have been designed and implemented by the author together with other members of Omega Verksted[1] [20] [21]. This is based on earlier designs by members of Omega Verksted, the last major implementation at Omega Verksted was done in 2009 mostly by Dewald de Bruyn.

[1] Omega Verksted is a association of electronics and hobby interested students at the Norwegian University of Science and Technology (NTNU) founded in 1971.

## 1.3 Overview

This thesis will begin by discussing an implementation of a DRSSTC, substantiating the functionality of sub circuits with mathematics. Then discuss the mathematical description of the resonant transformer, varying component sizes, plotting and simulating the transfer functions. Then present some measurements done on a physical implemented DRSSTC.

# Chapter 2

# DRSSTC

In a DRSSTC dual resonant means that we have two resonant circuits inductively coupled, and tuned to the same resonance frequency. Solid state means that we drive these resonant circuits actively with transistors. The origins of the DRSSTC is not well documented but it is commonly accepted that it was conceived on "The tesla coil mailing list" [1].

The signal pathway consists of a signal source, pulse limiter, power limiter, interrupter, amplifier, and power amplifier see fig. 2.1. The signal source provides a signal containing information on when the coil should fire, often the signal source is a musical recording. The input signal should be monophonic, arpeggio[1] may be used. The input signal may be two level.

First the input signal $X1$ goes into the pulse shaper, which transforms the signal to two level, limits on-time of each pulse, and enforces a minimum time between

[1]The sounding of the notes of a chord in rapid succession instead of simultaneously.

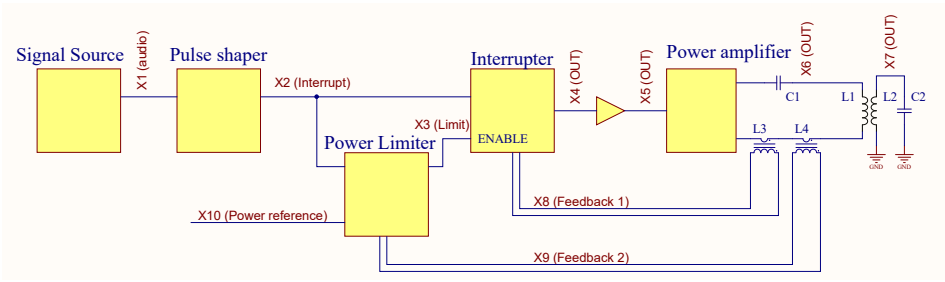


**Figure 2.1:** Block diagram

pulses. Then the signal $X2$ is connected to the interrupter which on a positive flank on $X2$ drives the resonant circuit at its resonant frequency until either the input pulse $X2$ goes low or the limit signal from the limiter $X3$ goes low. The limiter measures the current flowing through $C_1$ and $L_1$. If the current exceeds a preset level $X10$ the limit signal $X3$ is set low until the next rising edge of the input signal $X2$.

The resonant circuitry consists of $C_1$, $L_1$, $C_2$ and $L_2$, where $L_2$ is magnetically coupled with $L_1$.

## 2.1 Pulse shaper

The purpose of the pulse shaper is to take the input signal $X1$ and transform it to be suitable for a DRSSTC, in addition to not letting harmful signals through. The pulse shaper in this implementation is built separate from the driver. The first step in the pulse shaper is to transform the input signal $X1$ to two level as shown in fig. 2.2.

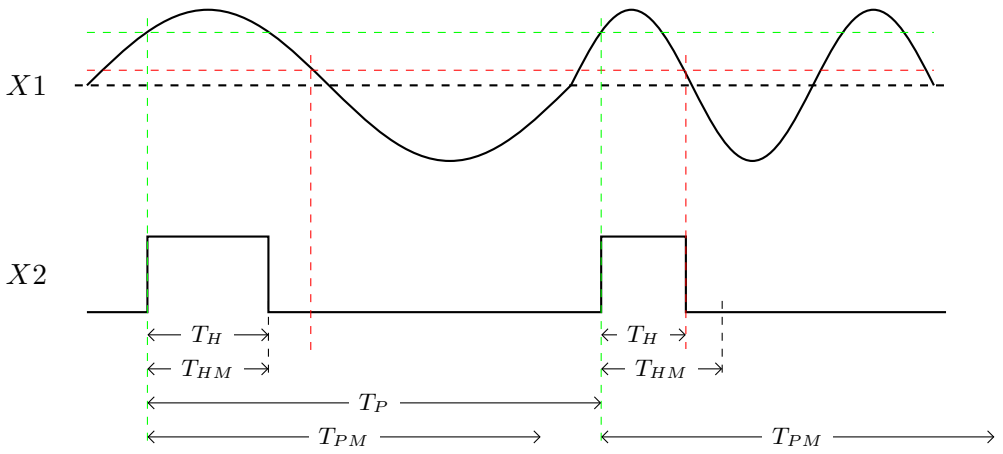


**Figure 2.2:** Detail view of signal $X2$

Here we see that the transformation to two level is done with a schmidt trigger, we also see that the pulse following immediately after the second pulse is suppressed wich will be explained below.

Then the triggering signal $X2$ is two level and contains two pieces of information from $X1$, the frequency $f_{X2}$ (tone) and the volume (intensity).

Where the frequency $f_{X2} = \frac{1}{T_P}$ is given by the time $T_P$ between the positive flanks of the signal. This is the base harmonic of the acoustic tone heard at the output

of the system. The volume is given by the duty cycle of the pulses $D = \frac{T_H}{T_P}$. Figure 2.3 shows different tones (varying $T_P$),

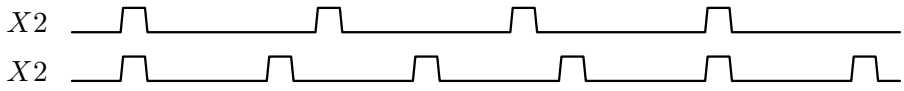


**Figure 2.3:** Different tones

and fig. 2.4 shows different volumes (varying $T_H$).

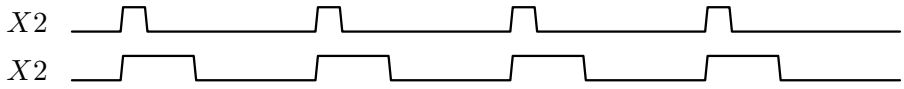


**Figure 2.4:** Different volumes

We also need to prevent harmful signals, meaning signals that may lead to destructive failure at the output. This is done by limiting the max duty cycle of the pulses as well as limiting the frequencies allowed. The duty cycle of the pulses is limited by choosing a maximum time $T_{HM}$ the pulse is allowed to be high, this time is independent of the frequency. This means the preset max duty cycle is dependent on the frequency of the pulse. Limiting the frequencies allowed is done by choosing a minimum time $T_{PM}$ after a pulse goes high until $X2$ is allowed to go high again.

How this can be implemented is not discussed any further in this thesis. But this thesis should give the basis for choosing maximum and minimum values for $T_H$ and $T_P$.

## 2.2 Interrupter

The interrupter generates the signal which drives the resonant circuit (coil rig) at its resonant frequency $f_0$. As long as the input signal $X2$ is high the output produces a square wave with fundamental frequency $f_0$. It does this by means of a positive feedback loop. The feedback signal $X8$ is retrieved with a sensing transformer around the output wire from the power amplifier (section 2.4), before being clamped, rectified, and schmidt triggered. This results in a cleaned up normalized representation of $X8$, lets call this signal $X8'$. The flanks of $X8'$ represents when the output current passes zero (this is when we want to switch the polarity of the output $X5$). $X8'$ is fed to the output via gates controlled by a latch. $X5\_B$ is inverted in relation to $X5\_A$ (for push-pull operation). This circuit is shown in fig. 2.5, U1A is the latch witch is central to the operation of the interrupter. It has Four inputs SD, CP, D, and RD, wich are 'Set Data' (active low), 'Clock Pulse', 'Data', and 'Reset Data' (active low) respectively. And two outputs; Q wich is the normal output, and Q inverted wich is the inverted of Q at all times, Q inverted is unused in this circuit.

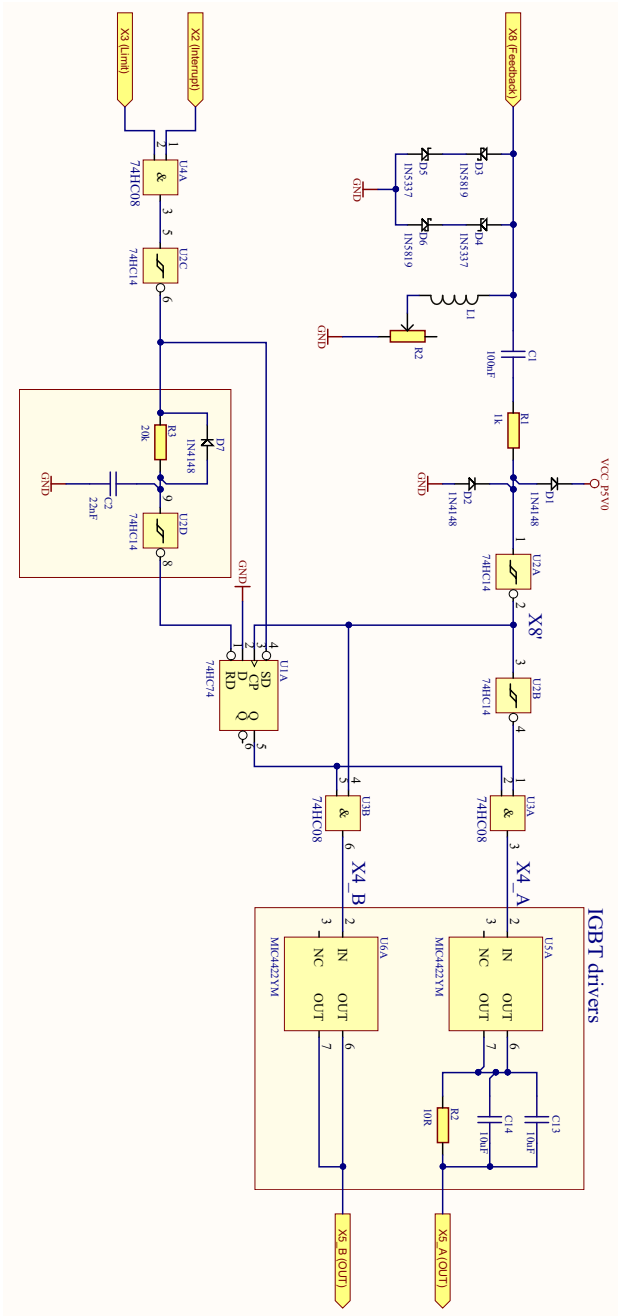


**Figure 2.5:** Interrupter (TK514)

Initially no current is flowing in the resonant circuit therefore no voltage is present on $X8$, but because of C1 the the input of U2A is undefined. Let us look at the case of the output of U2A being high and the input $X2$ being low. Then the initial values of the signals are as shown in fig. 2.6, SD is high (inactive) CP is high, D is low, RD is low (active), Q is low, $X4\_A$ and $X4\_B$ is low.

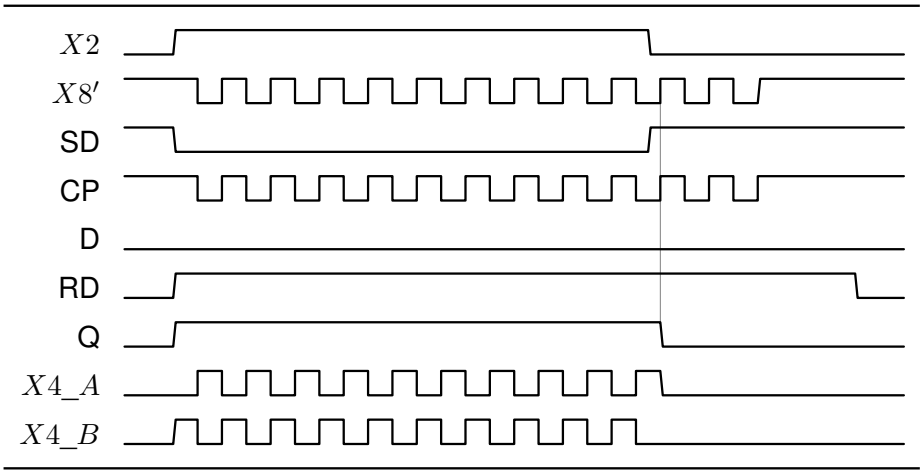


**Figure 2.6:** Timing diagram for interrupter

When $X2$ goes high the Set Data (SD) input of the latch U1A goes low and is activated, Reset Data RD goes high (inactive), and thus the output Q goes high. This enables the and gates U3A and U3B and allows X8' to pass through, $X4\_B$ goes high and $X4\_A$ remains low, this causes a step response in the resonant circuit. The feedback transformer is oriented such that this current direction gives a negative voltage on $X8$ and thus still low signal on the input of U2A. When the current direction changes the signal on the input of U2A goes from low to high and $X4\_A$ goes high and $X4\_B$ goes low. This reverses the voltage on the resonant circuit in phase with the step response and triggers an additional step response in phase with the already ongoing one. This cycle continues until $X2$ goes low. When $X2$ goes low SD goes low (inactive), but Q is still high until the next negative flank on $X8$ (inverted through U2A). When D (wich is strapped low) is clocked through the latch, Q goes low and both $X4\_A$ and $X4\_B$ goes low. And no further energy is supplied to the resonant circuit and the step response completes. In the case of the initial value of the output of U2A being low $X4\_A$ would go high first instead of $X4\_B$ and $X8$ would go high right away. Prompting $X4\_A$ and $X4\_B$ to invert immediately and switch the output while the current is not zero. Then the rest of the events happen as explained above. This immediate inverting of $X4$ may

be unfortunate and a pull down resistor should be added at the input of U2A. The resulting signal on the output $X7$ is then Pulse Density Modulated (PDM).

### Phase Lead

The function of $L_1$ and $R_2$ is to introduce a phase lead on the voltage of $X8$ in relation of the current on $X8$. The purpose of this is to compensate for propagation delays in the circuit and for switching delays in the transistors in the power amplifier (section 2.4). As the circuit is inductive, the voltage will lead the current. By adjusting the value of $R_2$ the relation between the inductance and resistance is changed and thus the phase angle is changed. Thus the time between when the voltage crosses zero and the current crosses zero can be adjusted. This time should theoretically be equal to the time it takes the feedback signal $X8$ to propagate through the logic and for the transistors (IGBTs) in the power amplifier to turn on or off. So that we will switch when the current in the resonant circuit is zero (Zero current switching). This is to reduce energy lost from the resonant circuit and to minimize power burned in the transistors (when switching). From the datasheets we have the propagation delays $t_{pd}$ for the different devices in the propagation path shown in table 2.1. The there are two propagation paths one path contains one schmidt trigger (74HC14) more than the other, also the propagation delay in the mosfet drivers (MIC4422YM) differs for rising and falling outputs. The average propagation delay $\overline{t_{pd}}$ from $X8$ on the input of U2A to $X5$ on the output of the mosfet drivers is then given by eq. (2.1) and results in $\overline{t_{pd}} = 58$ ns typical and 137,5 ns maximum.

| | Device | $t_{pd}$ Typ (ns) | $t_{pd}$ Max (ns) |
|---|---|---|---|
| $t_{inv}$ | 74HC14 | 12 | 25 |
| $t_{and}$ | 74HC08 | 10 | 20 |
| $t_{drivR}$ | MIC4422YM Rising | 20 | 80 |
| $t_{drivF}$ | MIC4422YM Falling | 40 | 80 |

**Table 2.1:** Propagation delays for devices

| | $T_J = 25°C$ | $T_J = 150°C$ |
|---|---|---|
| Turn-On Delay Time (ns) | 46 | 31 |
| Turn-Off Delay Time (ns) | 120 | 210 |

**Table 2.2:** Turn on and off delays in the IGBT IRG4PC50WPbF

$$\overline{t_{pd}} = t_{inv} + \frac{t_{inv}}{2} + t_{and} + \frac{t_{drivR} + t_{drivF}}{2} \tag{2.1}$$

In addition the delays from hysteresis in U2A $t_h$ and switching delays in the transistors in the power amplifier $t_{sw}$ should be added to the desired phase lead $t_d$. Resulting in the desired phase lead $t_d$ being given by eq. (2.2).

$$t_d = t_h + \overline{t_{pd}} + t_{sw} \tag{2.2}$$

The feedback signal $X8$ should have sufficiently high voltage so that delays from hysteresis $t_h$ in U2A is neglible. Delays in the IGBT is read from the datasheet and presented in table 2.2. If we add the delay at 25 $°C$ to the nominal $t_d$ and the delay at 150$°C$ to the maximum $t_d$, we get a $t_d$ of 141 ns nominal and 258 ns maximum.

Since there are no other resistances in the circuit than R2, as R1 is in series with both a capacitor and the input of the logic gate U2A and can be considered close to infinite in relation to R2, the phase angle is given by eq. (2.3).

$$\theta = \tan^{-1}\frac{X_{L_1}}{R_2} = \tan^{-1}\frac{\omega L_1}{R_2} = \tan^{-1}\frac{2\pi f_0 L_1}{R_2} \tag{2.3}$$

And thus the desired phase lead is given by eq. (2.4), and the relation between $L_1$ and $R_2$ is given by eq. (2.5).

$$t_d = \frac{\theta}{\omega} = \frac{\theta}{2\pi f_0} \tag{2.4}$$

$$\frac{L_1}{R_2} = \frac{\tan(\theta)}{\omega} = \frac{\tan(\omega t_d)}{\omega} = \frac{\tan(2\pi f_0 t_d)}{2\pi f_0} \tag{2.5}$$

Given $f_0$ = 110kHz and desired $t_d$ = 141 ns nominal and 258 ns maximum we get $\frac{L}{R} = 1,4 \cdot 10^{-7}$ s nominal and $\frac{L}{R} = 2,6 \cdot 10^{-7}$ s maximum. The total magnitude $|Z_L|$ of the impedance $Z_L$ of $L_1$ and $R_2$ should give a sufficiently high voltage $U_{X8}$ so that the delay due to hysteresis in U2A is negligible, but not too high voltage for the zener diodes D3-D6 to handle. The equation for $|Z_L|$ is shown in eq. (2.6).

$$|Z_L| = \sqrt{{R_2}^2 + (2\pi f_0 L_1)^2} \tag{2.6}$$

The relation between the peak voltage $|U_{X8}|$ over $R_2$ and $L_1$ is shown in eq. (2.7) assuming $X8$ is sinusiodal.

$$|U_{X8}| = |Z_L||I_{X6}|\frac{n1}{n2} \tag{2.7}$$

### Reset network

The function of the network connected to the reset (RD) of the latch (U1A) is to reset the latch after a delay in the case that a zero crossing is not detected on $X8$ after $X2$ goes low. Note the inverting schmidth triggers U2C and U2D on both sides of the network. When $X2$ goes high the input of U2D goes low immediately due to the capacitor $C_2$ being discharged through $D_7$, but when $X2$ goes low the capacitor $C_2$ will be charged through $R_3$ and there will be a delay before the latch is reset. The time constant of $R_3$ $C_2$ is $\tau = 440 \cdot 10^{-6}s$, the positive going threshold voltage of the inverting schmitt trigger (74HC14) is $T^+ = 2,5V$ Wich is half of the supply voltage VCC_P5V0. We know that a capacitor is charged to $0,5\cdot$ VCC (where VCC is the applied voltage) after $0,7\tau$, thus the filter $R_3$ $C_2$ together with U2D introduces a delay of $0,7\tau = 308\mu s$, or if we have a resonance frequency $f_0$ of 110 kHz a delay of about 3,4 periods $T = \frac{1}{f_0}$. If the synchronous shutdown does not work properly this filter should prevent or reduce noise from the interrupter not shutting down properly between each pulse on the input signal X2. This can also reduce the spark length if the spark is prevented from unintentionally continue longer than intended.

### Input clamping and protection

$D_3$-$D_6$ are protection diodes which clamp the feedback signal to safe voltages. The network $L_1$ and $R_2$ introduces a tunable phase lead on the voltage. $C_1$ and $R_1$ is a filter to remove noise. $D_1$ and $D_2$ clamps the voltage to 0-5V.

### IGBT Drivers

U5A and U6A are transistor drivers which amplify $X4$ and step up the voltage from 5V to 18V

## 2.3 Power Limiter

The limiter prevents overcurrent in the coil rig by disabling the interrupter when the peak current rises above a preset level. The limiter is shown in fig. 2.7

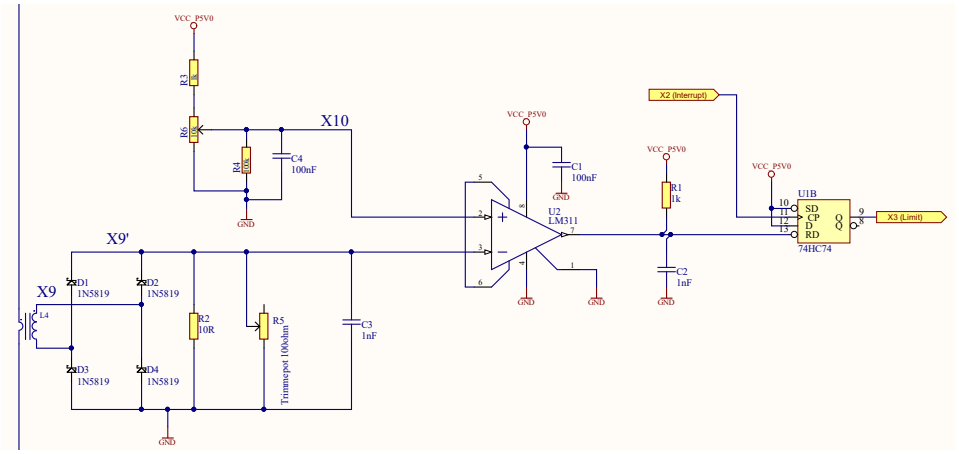


**Figure 2.7:** Limiter

The feedback signal is retrieved from the primary resonant circuit via the feedback transformer L4. The diodes D1-D4 is a full bridge rectifier, schottky diodes are used for low propagation delay. The rectifier is loaded with R2 and C3, R2 and C3 also functions as a noise filter with a cut off frequency $f_c$ given by eq. (2.8).

$$f_c = \frac{1}{2\pi R_2 C_3} \tag{2.8}$$

The cut off frequency $f_c$ decides how much noise is allowed through to the comparator and thus how often the spark is shut down early unintentionally due to noise. The spark being shut down unintentionally generates noise on the acoustic signal.

The rectified signal is fed into a comparator, the other input of the comparator is connected to a variable voltage controlled by a potentiometer. R3 is to set the highest level the variable voltage can be set to. R4 is to pull the input of the comparator low in the case that the potentiometer is disconnected.

The relation between the (peak) current in the primary resonance circuit and the (peak) voltage on the input of the comparator is given by eq. (2.9).

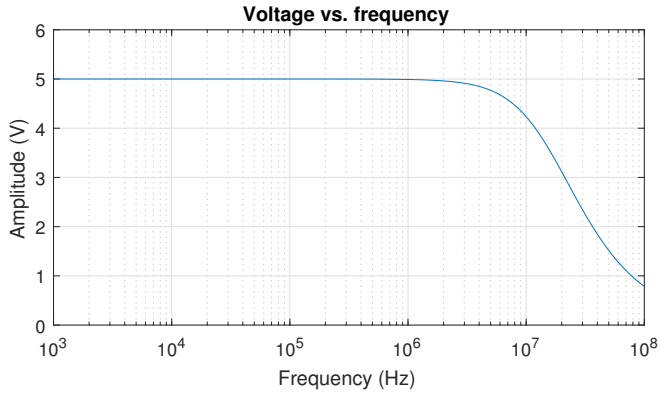


**Figure 2.8:** $I_1$=50A

$$\frac{U_{X9'}}{I_{X6}} = \frac{n_1}{n_2} \cdot \frac{R_2}{\sqrt{1 + (2\pi 2 f R_2 C_3)^2}} \tag{2.9}$$

Where $\frac{n_1}{n_2}$ is the winding ratio of the feedback transformer, $I_{X6}$ is the current running in the primary resonance circuit, $f$ is the fundamental frequency of $I_{X6}$ (half the frequency of the signal on the input of the comparator because of the full bridge rectifier). Given $n_1 = 1$, $n_2 = 100$, $R_2 = 10\Omega$, $C_3 = 1$nF, f = 110kHz, we get $\frac{U_{X9'}}{I_{X6}} = 0,1$ Volts per Ampere.

If the voltage of $X9'$ is higher than the voltage set by the potentiometer $X10$ the output of the comparator goes low and resets the latch. The data input of the latch is connected to VCC, on the next positive flank of the interrupt signal $X2$ the data will be clocked to the output and the output will go high.

$R_5$ is to give the possibility to tune the resistance of $R_2$ by removing $R_2$ from the PCB and mounting $R_5$ instead, $R_5$ then replaces $R_2$ in the calculations above.

$R_2$ decides the range of current that can be sensed and compared to the preset level. This is critical to the maximum amplitude attainable on the output and the range of amplitudes attainable. And thus affects the volume and dynamic range of the acoustic signal.

The output of the latch $X3$ is connected to the interrupter, as explained in section 2.2. A low signal stops the output of the interrupter. A high signal allows the interrupt signal $X2$ to control the output.

## 2.4 Power Amplifier

The purpose of the power amplifier is to amplify the signal coming from the interrupter $X5$ and drive the resonant circuit with a high voltage VCC_HVDC (section 2.6). The power amplifier is shown in fig. 2.9, note that the feedback transformer L4, as well as the secondary resonant circuit L2 and C2 is not shown for simplicity. The feedback transformer L3 is included in the figure.

The power amplifier is a full bridge inverter using Isolated Gate Bipolar Transistors (IGBTs), IGBTs are chosen over MOSFETs due to IGBTs having lower forward voltage drop at higher voltages and currents. The IGBTs are Q1 - Q4.The 1N4744A diodes (15V Zener) is there to clamp the gate voltage to protect the gate of the IGBT from over voltage. The 10 Ohm resistors is to protect from overcurrent. The 1V5KE400A schottky diodes are to protect the IGBTs from reverse voltage transients. The 15ETX06 diodes are there to recycle the leftover energy into the bus capacitors in the power supply when we have stopped switching, as IGBTs does not conduct reverse current. L3 is the current sense feedback transformer, L1 and C1 is the primary resonant circuit. T1 and T2 are gate drive transformers. The supply voltage VCC_HVDC is 160VDC.

### Gate drive transformers

T1 and T2 are gate drive transformers, the purpose of which is to isolate the low voltages in the interrupter from the higher voltages in the power amplifier, as well as to switch the phase for half of $X5$ the signal driving the transistors.

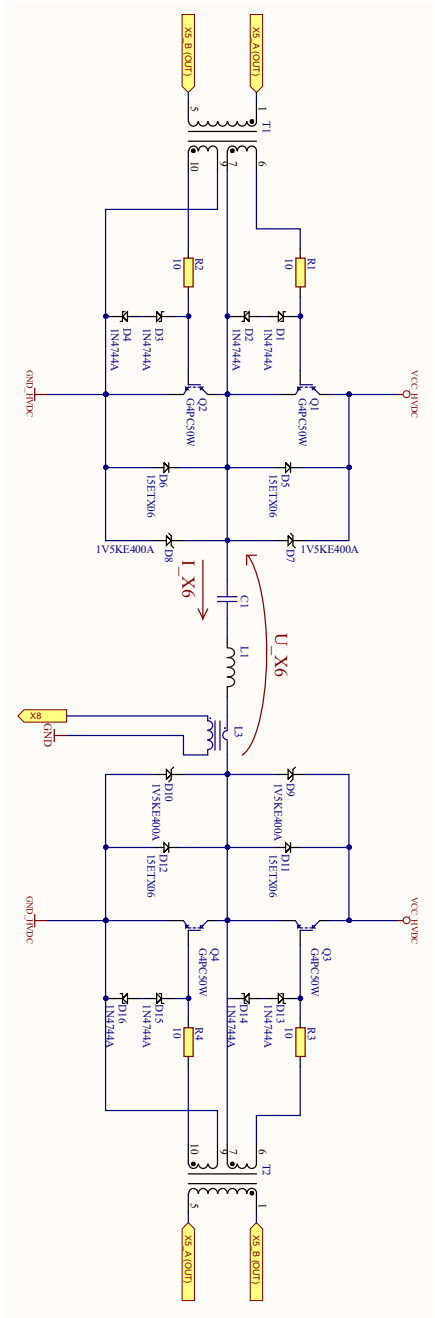


**Figure 2.9:** Power Amplifier

## 2.5 Coil rig

The coil rig steps up the voltage from VCC_HVDC to a voltage high enough to create electric arcs. The coil rig consists of two parts; the primary resonant circuit; $R_1$, $C_1$, $L1$, and the secondary resonant circuit; $L_2$, $R_2$, $C_2$, $G_1$. The resonant circuit is shown in fig. 2.10. The transfer function for the coil rig will be derived in section 3.1.

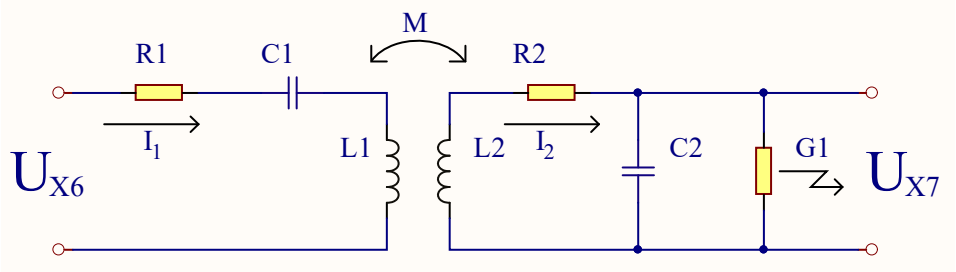


**Figure 2.10:** Resonant circuit

The input signal to the resonant circuit $X6$ is the square wave output from the power amplifier. When the interrupter first applies a voltage to the primary resonant circuit through the power amplifier the circuit responds with its step response on the output $U_{X7}$ and current $I_1$ (shown in fig. 3.5 and fig. 3.10), this is a damped sinusoidal and with a frequency equal to the resonant frequency. When the interrupter detects that the current in the primary resonant circuit $I_1$ passes zero the polarity switches, as explained in section 2.2, and we get a new step response added to the already existing one. This continues for several cycles. This current is inductively coupled into the secondary resonant circuit, and when the voltage reaches a high enough level an electric discharge happens from the top load of the secondary resonant circuit, this drains energy from the secondary circuit, but the electric discharge continues to grow for a couple of cycles. The wave forms of the signals will be explained in chapter 3.

The values and the physical shapes of the components in the resonant circuit are important to the operation of the tesla coil. The values of the components will be discussed in chapter 3. A photo of a coil rig is shown in fig. 2.11.

$L_1$ is the primary coil, and will have few turns and large area. It is important that $L_1$ is constructed such that $k$ is $0.2$ and so that we wont get any arcing from $L_1$ to $L_2$. This can be achieved by using a conical coil or a flat spiral coil (in fig. 2.11 a conical coil is shown). The inductance of $L_1$ can be calculated from eq. (2.10) and fig. 2.12 if a conical coil is used.

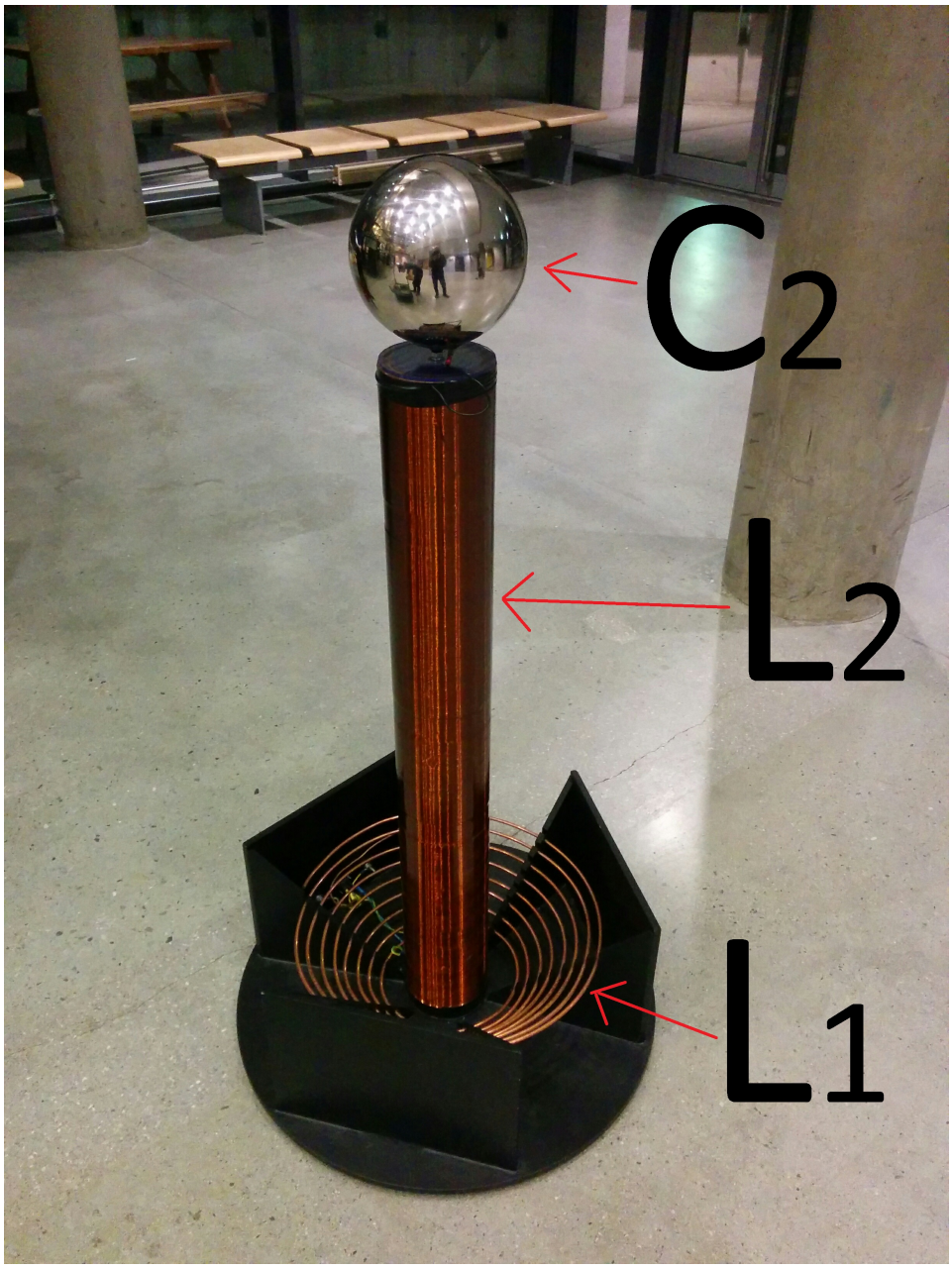


**Figure 2.11:** Image of a coil rig

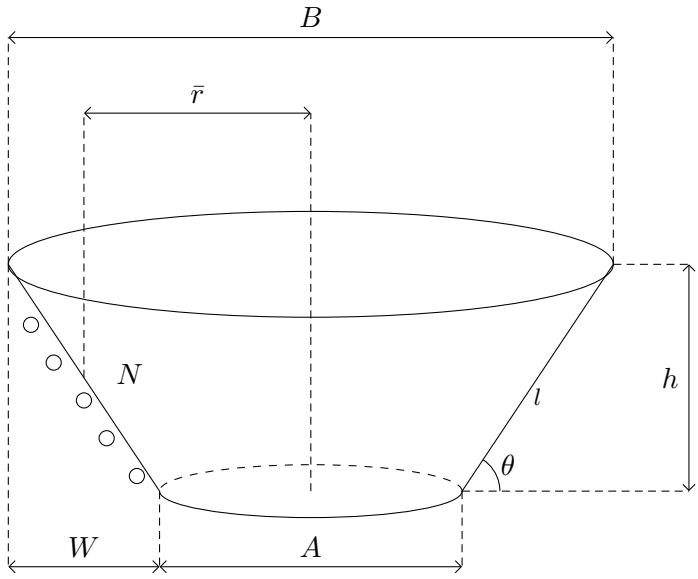


**Figure 2.12:** Conical coil

$$L_1 = \sqrt{(L_{1V} \cdot \sin(\theta))^2 + (L_{1H} \cdot \cos(\theta))^2} \tag{2.10}$$

$$L_{1V} = \frac{R^2 N^2}{9\bar{r} + 10h}, L_{1H} = \frac{R^2 N^2}{8\bar{r} + 11h} \tag{2.11}$$

$$\bar{r} = \frac{A}{2} + \frac{W}{2} \tag{2.12}$$

$$\sin(\theta) = \frac{h}{l}, \cos(\theta) = \frac{W}{l} \tag{2.13}$$

$$l = \sqrt{W^2 + h^2} \tag{2.14}$$

$$W = \frac{B - A}{2} \tag{2.15}$$

$h$ is height of cone, $B$ diameter top of cone, $A$ diameter base of cone, $N$ number of turns, $\bar{r}$ is effective with of coil $l$ is length of coil, $\theta$ is angle of coil, $L_{1V}$ is the

vertical component of the inductance, $L_{1H}$ is the horizontal part of the inductance. This equation comes from the empirical wheeler equations [18].

$L_2$ is the secondary coil and will have many turns and small area. This has the form of a solenoid with a single layer of windings. The inductance of $L_2$ can be found with eq. (2.16).

$$L_2 = \frac{\mu_0 N^2 \pi r^2}{l} \tag{2.16}$$

Where $\mu_0$ is permeability for vacuum, $N$ is the number of turns, and $l$ is the length of the coil. This equation comes from the long solenoid approximation.

$C_1$ is an ordinary capacitor, the type of capacitor should be chosen to withstand the voltages and current required without degrading. And should have as low resistance as possible.

$C_2$ is the place where we want the electric discharge to happen, and thus $C_2$ must withstand the voltages and currents required without degrading. This is achieved by using the self capacitance of a single conductor as opposed to the more common mutual capacitance of two paralell plates. $C_2$ is placed at the top of $L_2$ and is also known as the top load, the top load can be any shape that does not have sharp corners. The most common shapes are spherical or toroidal. The self capacitance of a spherical top load $C_2$ is given by eq. (2.17).

$$C_2 = 4\pi\epsilon_0 r_c \tag{2.17}$$

Where $\epsilon_0$ is the permittivity of vacuum, and $r_c$ is the radius of the sphere. This equation is derived from the capacitance of an spherical paralell plate capacitor where the radius of the outer sphere goes toward infinity.

## 2.6 Power supply

The power supply for the driver is, as for most electronic systems, critical for the quality of operation. This implementation uses three different power supplies for VCC_P5V0, VCC_P18V, and VCC_HVDC. Wich are 5,0V DC, 18V DC, and 160V DC respectively. VCC_P5V0 supplies the logic circuits, and should supply enough power for this, as well as not introducing noise to the signals in the logic circuits. VCC_P18V supplies power to the transistor drivers in the interrupter, and has the same requirements as VCC_P5V0. VCC_HVDC supplies the power amplifier, and should be able to supply large peak currents with low resistance and delay, as seen from the simulation of the current drawn by the primary resonant

circuit in fig. 3.12 in section 3.2. How this can be achieved is assumed well understood and documented in the field of electronics and will not be discussed any further.

## 2.7 Shielding

The electric discharge produced by a tesla coil generates a large dynamic electromagnetic field. This will induce currents in any conductor close to the tesla coil. This must be taken into account when doing pcb layout and designing the chassis for the tesla coil driver. How this can be achieved is assumed well understood and documented in the field of electronics and electrodynamics and will not be discussed any further.

## 2.8 Optical channel

As mentioned in section 2.7 there is electromagnetic noise present when the tesla coil is used and a robust channel is needed for signal $X2$ because this signal is transmitted from the pulse shaper to the tesla coil driver, wich as mentioned in section 2.1 are physically located in different chassis some distance apart. For this plastic optical fibre is chosen. To further increase the robustness the signal $X2$ is modulated. The robustness and possible noise introduced in this channel is not discussed further as it can be treated as an isolated problem and is assumed well understood and documented in the field of electronics. A diagram of the optical channel is shown in fig. 2.13.

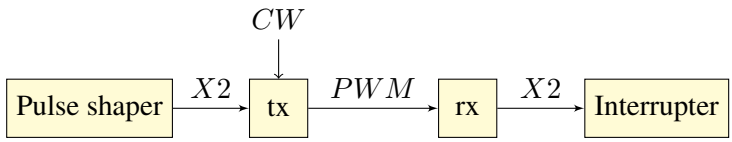


**Figure 2.13:** Diagram of optical channel

Where CW is the carrier wave used to modulate the signal $X2$, PWM is the modulated signal $X2$. The blocks tx and rx are the optical transmitter and reciever.

# Chapter 3

# Mathematical model

To better understand the load of the driver, which is the coil rig, we will look at a mathematical description of the coil rig. With a better understanding and good mathematical description of the coil rig the reader should be better suited to improve or adapt the driver.

## 3.1 Transfer function for coil rig

The schematic shown in fig. 3.1 is the schematic for the coil rig.

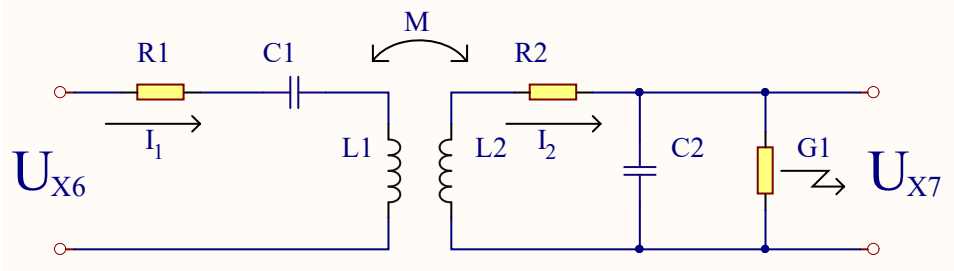


**Figure 3.1:** Coil rig

$R_1$ is the resistance in the primary circuit (mainly the cable from the driver to the coil rig), $R_2$ is the resistance in the secondary circuit (mainly the resistance in $L_2$). $C_1$ is the primary capacitor, $L_1$ is the primary coil, $L_2$ is the secondary coil, and $C_2$ is the secondary capacitance (or top load). $G_1$ is the electrical arc modelled as a conductance, see eq. (3.34) for the model of $G_1$, this model is a combination of Cassie [3] and Mayr [10] models for electrical arcs presented in [14]. $U_{X6}$ is the voltage output from the driver to the primary resonant circuit, $U_{X7}$ is the voltage

output from the secondary resonant circuit (the voltage driving the electrical arc).

This schematic can be simplified by introducing the mutual inductance $M$ as a component as shown in fig. 3.2.

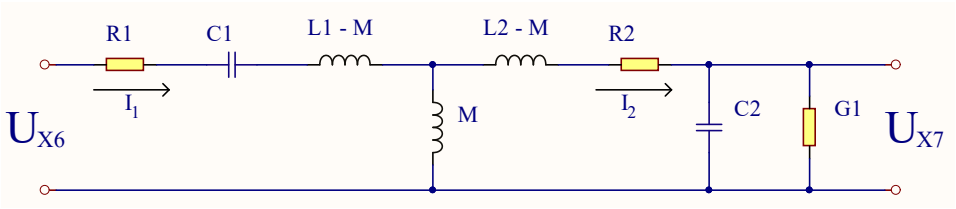


**Figure 3.2:** Coil rig simplified

And then further simplified by representing the branches of the circuit as impedances as shown in fig. 3.3.

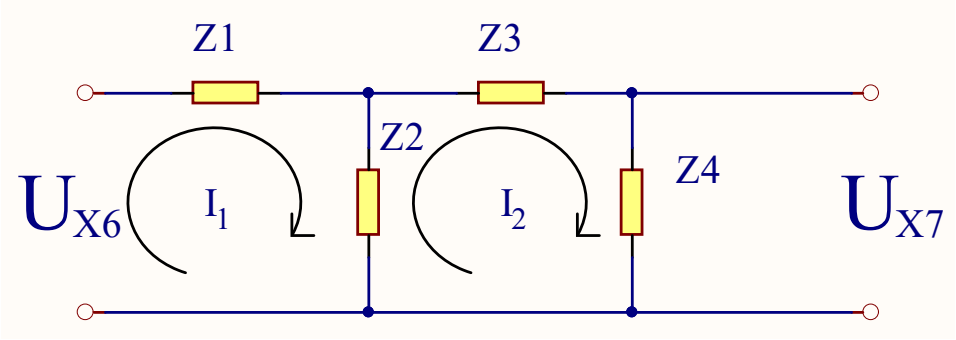


**Figure 3.3:** Coil rig represented with impedances

Using the mesh current method we get eq. (3.1) and eq. (3.2).

$$U_{X6} - I_1 Z_1 - (I_1 - I_2) Z_2 = 0 \tag{3.1}$$

$$(I_2 - I_1) Z_2 - I_2 Z_3 - I_2 Z_4 = 0 \tag{3.2}$$

We then solve these two equations for $I_1$. Set eq. (3.4) equal to eq. (3.5), solve for $\frac{U_{X7}}{U_{X6}}$ and substitute in eq. (3.3).

$$U_{X7} = I_2 Z_4 \tag{3.3}$$

$$I_1 = \frac{U_{X6} + I_2 Z_2}{Z_1 + Z_2} \tag{3.4}$$

,

$$I_1 = \frac{(Z_2 - Z_3 - Z_4) I_2}{Z_2} \tag{3.5}$$

We then have the transfer function $H(s)$ for the coil rig eq. (3.6).

$$\frac{U_{X7}}{U_{X6}} = H(s) = \frac{Z_2 \cdot Z_4}{Z_1 \cdot (Z_2 - Z_3 - Z_4) - Z_2 \cdot (Z_3 + Z_4))} \tag{3.6}$$

where

$$Z_1 = R_1 + \frac{1}{sC_1} + sL_1 - sM, \tag{3.7}$$

$$Z_2 = sM, \tag{3.8}$$

$$Z_3 = sL_2 - sM + R_2, \tag{3.9}$$

$$Z_4 = \frac{1}{sC_2} + \frac{1}{G_1}, \tag{3.10}$$

$$M = k\sqrt{L_1 L_2}. \tag{3.11}$$

However to be able to analyze this transfer function we have to order it into standard form. Meaning isolating $s$,$s^2$,$s^3$ etc. and expanding the factors. This leads to eq. (3.12).

$$H(s) = \frac{s^3 f + s^2 g}{s^4 a + s^3 b + s^2 c + sd + e} \tag{3.12}$$

where

$$a = (C_1 C_2 G_1 L_1 L_2) - 2(C_1 C_2 G_1 L_1 M) + (C_1 C_2 G_1 M^2), \tag{3.13}$$

$$b = (C_1C_2G_1L_1R_2)+(C_1C_2G_1L_2R_1)-2(C_1C_2G_1MR_1)+(C_1C_2L_1), \quad (3.14)$$

$$c = (C_1C_2G_1R_1R_2) + (C_1C_2R_1) + (C_1G_1L_1) + (C_2G_1L_2) - 2(C_2G_1M), \quad (3.15)$$

$$d = (C_1G_1R_1) + (C_2G_1R_2) + C_2, \quad (3.16)$$

$$e = G_1, \quad (3.17)$$

$$f = C_1C_2M, \quad (3.18)$$

and

$$g = C_1G_1M. \quad (3.19)$$

Orders of magnitude for the parameters in the transfer function is shown in table 3.1 these sizes are rounded approximate sizes for a DRSSTC, and are found from the implementation of Omega Verksted [20].

| | Comment | | |
|---|---|---|---|
| C1 | Primary load capacitor | $10^{-7}$ | F |
| C2 | Secondary load capacitor (top load) | $10^{-11}$ | F |
| L1 | Primary coil | $10^{-5}$ | H |
| L2 | Secondary coil | $10^{-1}$ | H |
| M | Mutual inductance | $2 \cdot 10^{-4}$ | H |
| R1 | Primary circuit ohmic resistance | $10^{0}$ | $\Omega$ |
| R2 | Secondary circuit ohmic resistance | $10^{2}$ | $\Omega$ |
| G1 | Minimum conductance of electrical arc | $2 \cdot 10^{-6}$ | $\Omega - 1$ |
| k | Coupling factor | $2 \cdot 10^{-1}$ | |

**Table 3.1:** Model parameter sizes

Shown in fig. 3.4 is the bode plot of the transfer function $H(s)$ eq. (3.12) of the resonant circuit with the orders of magnitude in table 3.1. Where the value for $G_1$ is the minimum conductance possible when there is no electrical discharge.

With electrical discharge (streamer or corona) the conductance will increase. The figures in this section is generated with Matlab and the code used to generate them can be found in appendix A

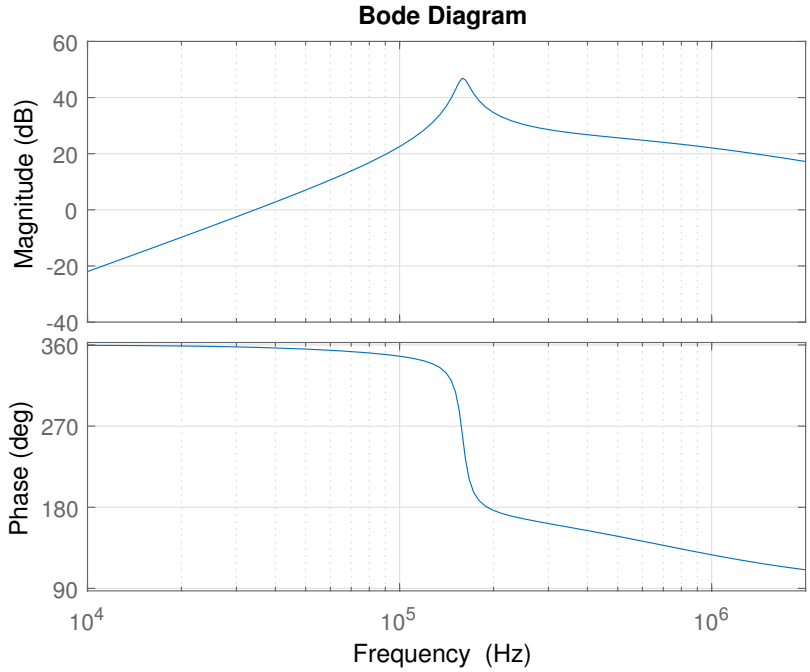


**Figure 3.4:** Bode plot of $H(s)$

We would expect a resonance frequency given by eq. (3.20) and table 3.1 of $f_0 = 160$kHz. Here we see that the resonance frequency in fig. 3.4 is $f_0 = 157$kHz, this is close to the expected. The magnitude at resonance is 47dB. We also see a steeper slope at frequencies lower than $f_0$ than above $f_0$.

$$f_0 = \frac{1}{2\pi\sqrt{L_1 C_1}} \tag{3.20}$$

$$Q = \frac{f_0}{BW} = \frac{X}{R} = \frac{2\pi f L_1}{R_1} \tag{3.21}$$

Where $BW$ is the bandwidth.

In fig. 3.5, we see the step and impulse responses of the transfer function $H(s)$ for the resonant circuit.

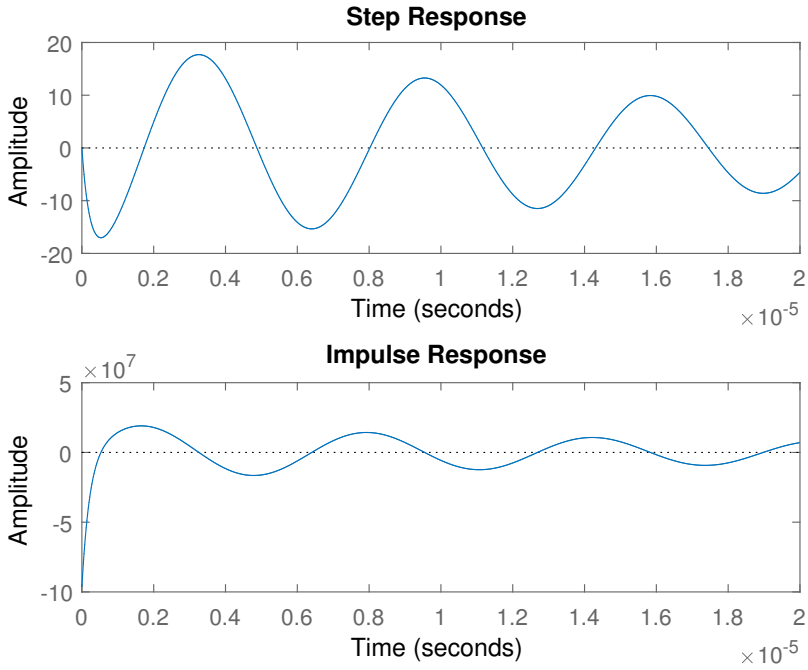


**Figure 3.5:** Step and impulse response for $H(s)$

Here we see that we have a damped sinusiodal response with a frequency $f_s$ of 156kHz witch is the same frequency as the resonance frequency $f_0$ of the frequency response. This response attenuates within a few cycles.

Figure 3.6 shows the poles and zeros of the transfer function $H(s)$ of the resonant circuit in angular frequency.

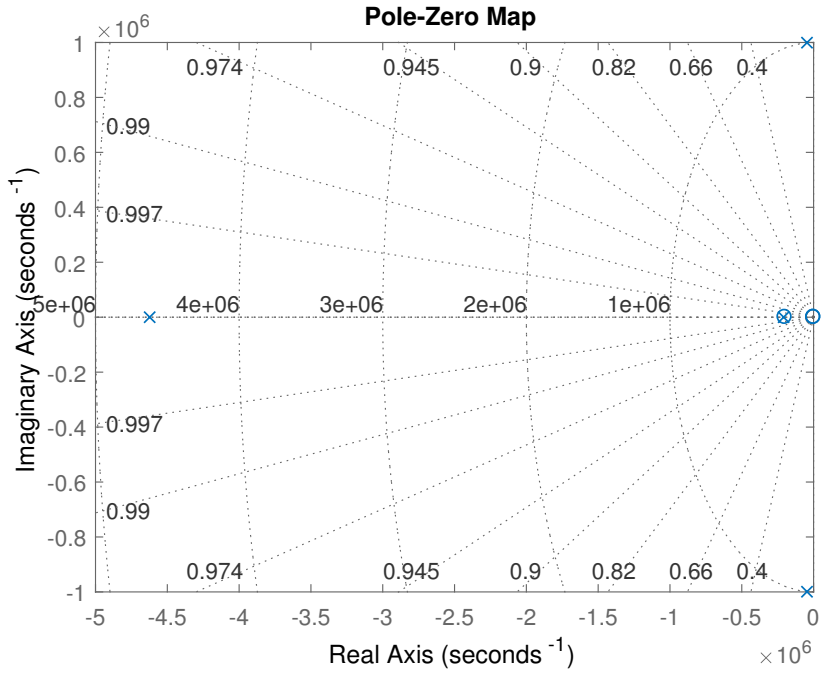


**Figure 3.6:** PoleZeroPlot for $H(s)$ in angular frequency

Table 3.2 shows the numerical values of the poles and zeros of the transfer function $H(s)$ of the resonant circuit in angular frequency.

| Poles | Zeros |
|---|---|
| $(-46 + 0i) \cdot 10^5 s^{-1}$ | |
| $(-0,4 + 9,9i) \cdot 10^5 s^{-1}$ | $0$ |
| $(-0,4 - 9,9i) \cdot 10^5 s^{-1}$ | $0$ |
| $(-2,1 + 0i) \cdot 10^5 s^{-1}$ | $-2 \cdot 10^5 s^{-1}$ |

**Table 3.2:** Poles and zeros for $H(s)$ in angular frequency

Here we observe a complex conjugated pole pair in the left half plane close to the imaginary axis, a single pole on the real axis far in the left half plane, a pole and a zero on the real axis close to origo, as well as two zeros in origo. From this we can say that the system is dominated by the complex pole pair and the zeros in origo. The pole and zero at the same place will cancel each other, and since the last pole is far to the left in relation to the complex pole pair, over four times as far out on

the real axis at -46, than the complex pole pair is on the complex axis at $\pm 9, 9$. It will have an effect but not dominating. A complex pole pair together with two zeros in origo implies a high pass filter, this does not matc well with the frequency response. The closer to the imaginary axis the pole pair is the higher the magnitude in the frequency response. This is consistent with the desired functionality. The pole far out on the real axis will give positive (higher magnitude) contribution that is at maximum in origo and reduces when the frequency increases, this makes the response closer to a band pass filter witch is consistent with the frequency response.

Figure 3.7 shows the result of a linear simulation of the transfer function of the resonant circuit with a square wave input signal with amplitude 160V peak and frequency 159kHz.

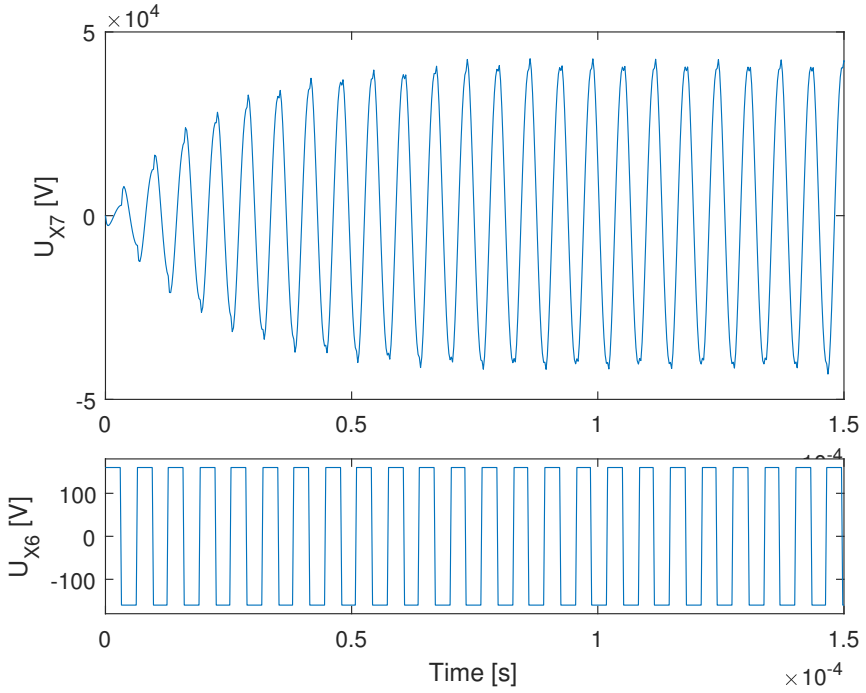


**Figure 3.7:** Linear simulation of transfer function $H(s)$ with square wave $X6$ with $f = f_0$ as input, and $X7$ is output

We see here that the output signal $X7$ starts with a quarter period of the step response shown in fig. 3.5, and then when the voltage peaks, meaning when the differential of the voltage is zero, a new step response with opposite phase is added

to the output signal. This makes the output signal grow rapidly for ten cycles before flattening out at 427kV.

Figure 3.8 shows the same simulation as fig. 3.7, but here the input signal is set to zero after 10 periods.

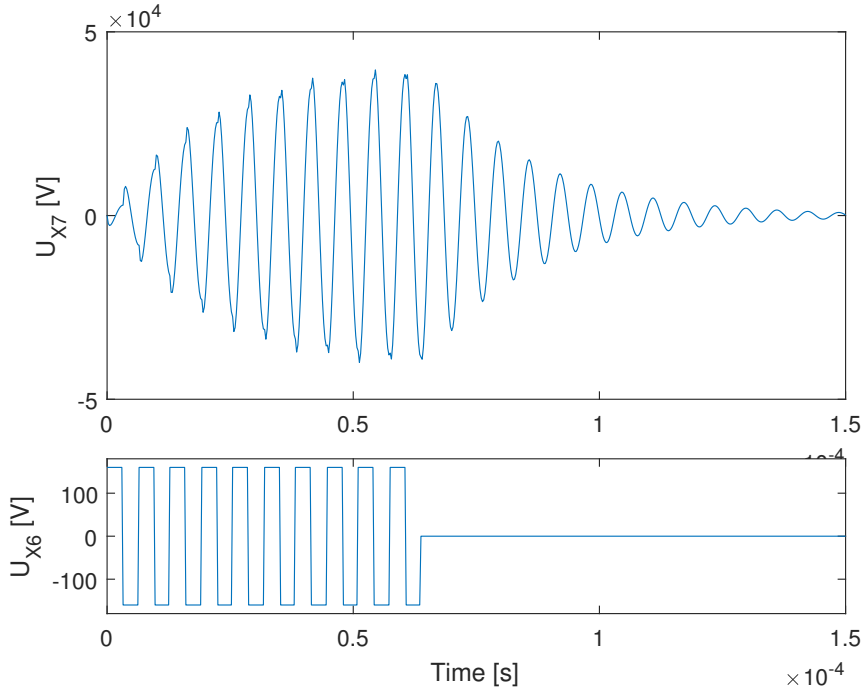


**Figure 3.8:** Linear simulation of transfer function $H(s)$ with 10 periods square wave $X6$ with $f = f_0$ as input, and $X7$ is output

Here we see that the voltage continues to resonate after the input is set to zero, but attenuates exponentially.

## 3.2 Transfer function for primary current I1

If we use eq. (3.1) and eq. (3.2) and solve for $\frac{I_1}{U_{X6}}$ we get the transfer function for the current flowing in the primary resonant circuit $I_1$ this is the signal that is coupled to the feedback signals $X8$ and $X9$ with current sense transformers $L_3$ and $L_4$. This is transfer function $H_{FB}$ is shown in eq. (3.22). Where $Z_1$ to $Z_4$ are the same impedances as given in eq. (3.6).

$$\frac{I_1}{U_{X6}} = H_{FB}(s) = \frac{Z_2 - Z_3 - Z_4}{(Z_1 + Z_2)(Z_2 - Z_3 - Z_4) - Z_2^2} \tag{3.22}$$

$$H_{FB}(s) = \frac{s^3 h + s^2 k + sl}{s^4 m + s^3 n + s^2 o + sp + q} \tag{3.23}$$

Where

$$h = 2(C_1 C_2 G_1 M) - (C_1 C_2 G_1 L_2) \tag{3.24}$$

$$k = -(C_1 C_2 G_1 R_2) - (C_1 C_2) \tag{3.25}$$

$$l = -C_1 G_1 \tag{3.26}$$

$$m = (C_1 C_2 G_1 L_1 L_2) - 2(C_1 C_2 G_1 L_1 M) \tag{3.27}$$

$$n = (C_1 C_2 G_1 L_1 R_2) + (C_1 C_2 L_1) + (C_1 C_2 G_1 R_1 L_2) - 2(C_1 C_2 G_1 R_1 M) \tag{3.28}$$

$$o = (C_1 G_1 L_1) + (C_1 C_2 R_1) + (C_2 G_1 L_2) - 2(C_2 G_1 M) \tag{3.29}$$

$$p = (C_1 G_1 R_1) + (C_2 G_1 R_2) + C_2 \tag{3.30}$$

$$q = G_1 \tag{3.31}$$

Figure 3.9 Shows the bode plot for the transfer function $H_{FB}(s)$.

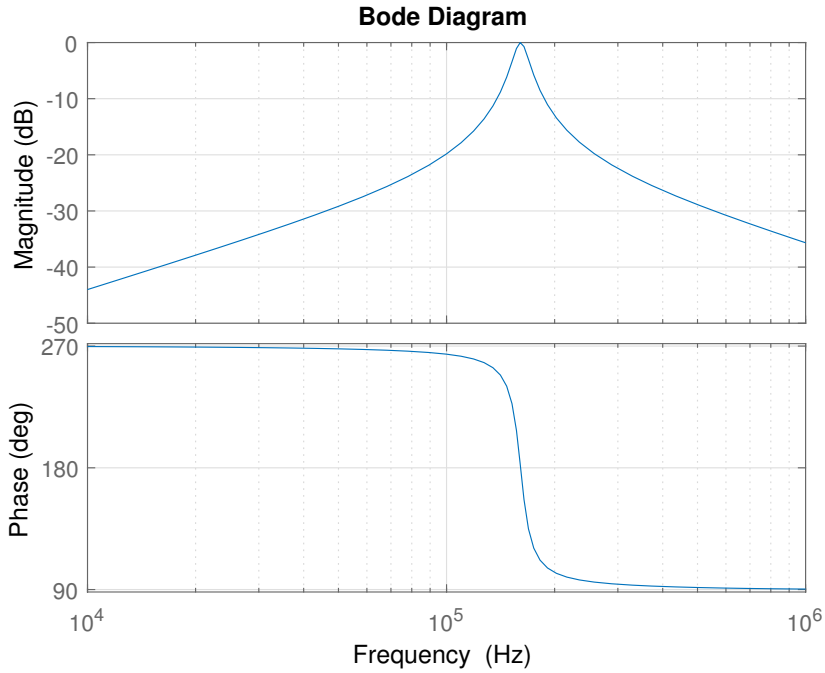


**Figure 3.9:** Bode plot of the transfer function for the feedback signals $H_{FB}(s)$

Here we see a much sharper peak at the resonant frequency than in the bode plot for the resonant circuit $H(s)$. We also see that the response is not less steep at frequencies higher than the resonance frequency. The resonant frequency $f_0$ is 160kHz and the magnitude is 0dB at resonance.

Figure 3.10 shows the step and impulse response of the feedback transfer function $H_{FB}(s)$.

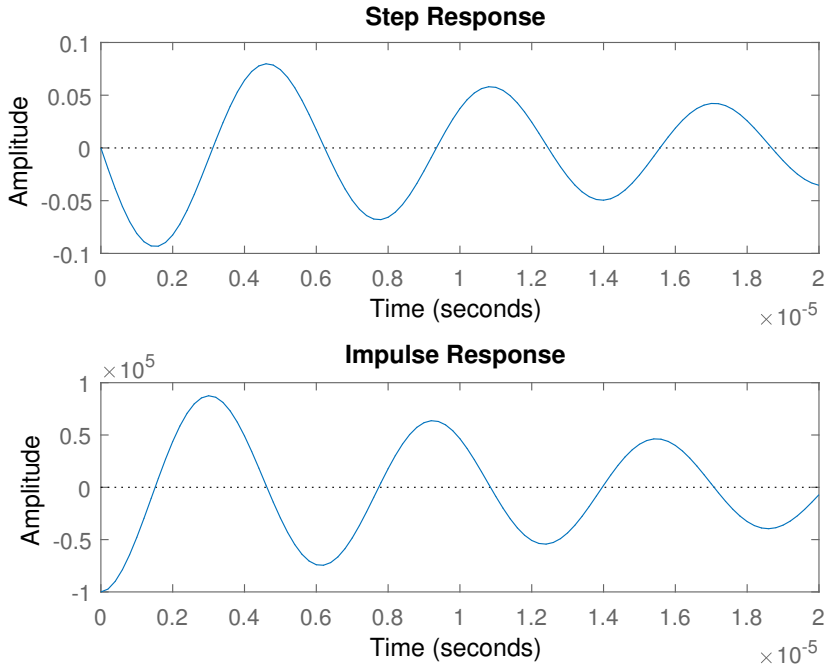


**Figure 3.10:** Step and impulse response of transfer function for the feedback current

Here we see a damped sinusoiodal response with a frequency $f_s$ of 167kHz witch is slightly higher than the resonant frequency $f_0$ of 160kHz. The step response of the feedback signal attenuates slower than the step response of the resonant circuit.

Figure 3.11 shows the pole and zero plot for the transfer function for the feedback signals $H_{FB}(s)$ in angular frequency.

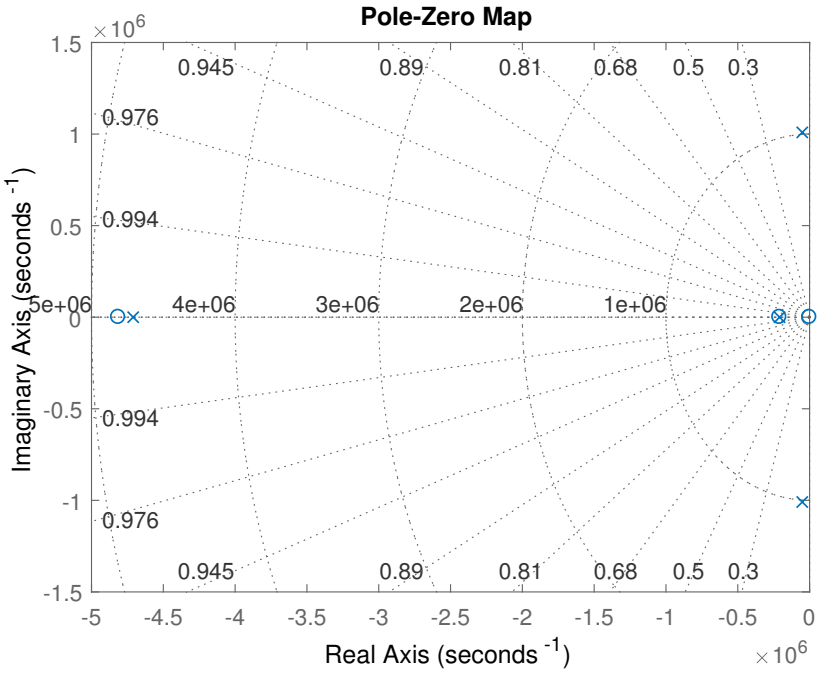


**Figure 3.11:** PoleZeroPlot for $H_{FB}(s)$ in angular frequency

Table 3.3 shows the numerical values of the poles and zeros of the transfer function for the feedback signals $H_{FB}(s)$ in angular frequency.

| Poles | Zeros |
|---|---|
| $(-47 + 0i) \cdot 10^5 s^{-1}$ | |
| $(-0,5 + 10i) \cdot 10^5 s^{-1}$ | $0$ |
| $(-0,5 - 10i) \cdot 10^5 s^{-1}$ | $-48 \cdot 10^5 s^{-1}$ |
| $(-2,1 + 0i) \cdot 10^5 s^{-1}$ | $-2,1 \cdot 10^5 s^{-1}$ |

**Table 3.3:** Poles and zeros for $H_{FB}(s)$ in angular frequency

Here we observe a complex conjugated pole pair in the left half plane, two real poles in the left half plane. As well as three zeros, two in the left half plane and one in origo. We see that the pole and zero close to origo cancel each other, but the pole and zero further to the left does not completely cancel out. This system is dominated by the complex conjugated pole pair together with the zero in origo. The pole and zero far to the left will have little effect. This implies a band pass

filter, the complex conjugated poles are close to the imaginary axis which gives a higher magnitude and is consistent with the desired functionality.

Figure 3.12 shows the result of a linear simulation of the transfer function of the feedback signal with a 160V peak square wave input signal with amplitude 1 and frequency 159kHz.

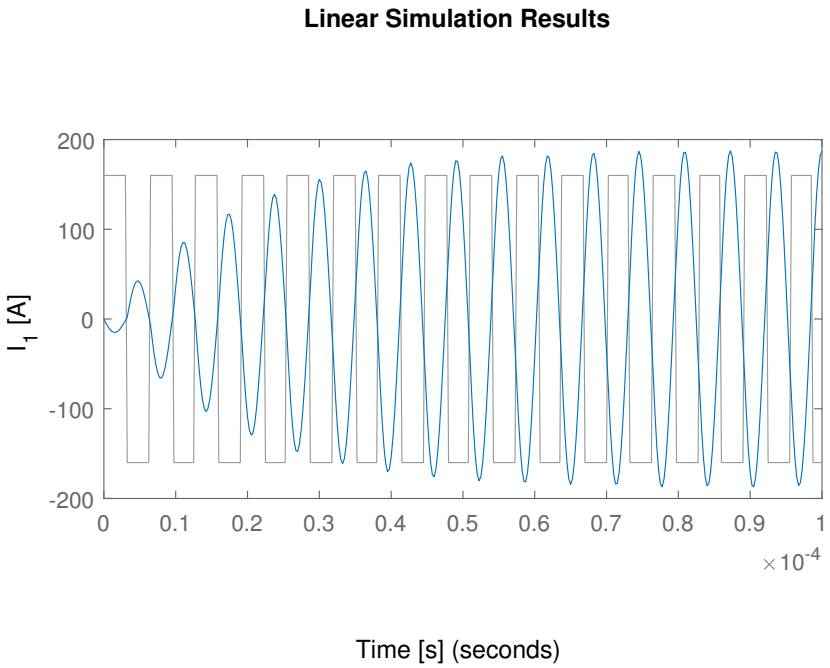


**Figure 3.12:** Linear simulation of transfer function with square wave with $f = f_0$ as input

Here we see a sinusoidal current that grows rapidly for 9 cycles to 182A then stabilizes at 186A. We also see that the input signal switches when the current is zero, though after some cycles the input signal drifts out of sync with the current.

## 3.3 Magnitude analysis

By taking the magnitudes for each variable listed in table 3.1 and inserting them into the different terms in the transfer function $H(s)$ (eq. (3.6)) we can see witch terms influence the result and witch terms are insignificant. In table 3.4 the values of each of the terms making up the main terms in eq. (3.6), are listed after inserting the magninudes in table 3.1. e, f, and g are not listed since they only have a single term each.

| | | |
|---|---|---|
| a | $(C_1C_2G_1L_1L_2)$ | $2 \cdot 10^{-29}$ |
| | $2(C_1C_2G_1L_1M)$ | $8 \cdot 10^{-32}$ |
| | $(C_1C_2G_1M^2)$ | $8 \cdot 10^{-31}$ |
| b | $(C_1C_2G_1L_1R_2)$ | $2 \cdot 10^{-26}$ |
| | $(C_1C_2G_1L_2R_1)$ | $2 \cdot 10^{-23}$ |
| | $2(C_1C_2G_1MR_1)$ | $8 \cdot 10^{-26}$ |
| | $(C_1C_2L_1)$ | $1 \cdot 10^{-23}$ |
| c | $(C_1C_2G_1R_1R_2)$ | $2 \cdot 10^{-20}$ |
| | $(C_1C_2R_1)$ | $1 \cdot 10^{-17}$ |
| | $(C_1G_1L_1)$ | $2 \cdot 10^{-17}$ |
| | $(C_2G_1L_2)$ | $2 \cdot 10^{-17}$ |
| | $2(C_2G_1M)$ | $8 \cdot 10^{-20}$ |
| d | $(C_1G_1R_1)$ | $2 \cdot 10^{-11}$ |
| | $(C_2G_1R_2)$ | $2 \cdot 10^{-14}$ |
| | $C_2$ | $1 \cdot 10^{-11}$ |

**Table 3.4:** Magnitudes of parameters in H(s)

From table 3.4 we see that the first term of $a$ is the largest, and the second and third terms are two and one orders smaller. Thus they are not significant and can be removed without reducing accuracy significantly. Further the first and third terms of $b$ are three orders smaller than the second and fourth terms and can be removed with the same reasoning. The second and fourth terms of $b$ are of the same magnitude and is thus equally significant. Two terms can be removed from $c$ and one term from $d$. e, f, and g only contains one term each and can not be simplified. This gives the simplified main parameters shown in eq. (3.32) and eq. (3.33).

$$a' = (C_1C_2G_1L_1L_2), b' = [(C_1C_2G_1L_2R_1) + (C_1C_2L_1)], \tag{3.32}$$

$$c' = [(C_1C_2R_1) + (C_1G_1L_1) + (C_2G_1L_2)], d' = [(C_1G_1R_1) + C_2] \tag{3.33}$$

Inserting the magnitudes from table 3.1 in $H(s)$ both before and after simplifying gives the same result when rounded to one significant digit as shown in table 3.5.

| | Before | After |
|---|---|---|
| a | $2 \cdot 10^{-29}$ | $2 \cdot 10^{-29}$ |
| b | $3 \cdot 10^{-23}$ | $3 \cdot 10^{-23}$ |
| c | $5 \cdot 10^{-17}$ | $5 \cdot 10^{-17}$ |
| d | $3 \cdot 10^{-11}$ | $3 \cdot 10^{-11}$ |
| e | $2 \cdot 10^{-05}$ | $2 \cdot 10^{-05}$ |
| f | $2 \cdot 10^{-22}$ | $2 \cdot 10^{-22}$ |
| g | $4 \cdot 10^{-16}$ | $4 \cdot 10^{-16}$ |

**Table 3.5:** Terms in H(s) before and after magnitude analysis with one significant digit

## 3.4 Streamer

When the electric discharge from the top load of the resonant circuit forms long threads or filaments in the air this is called a streamer discharge [19]. When a streamer discharge happens this affects the resonant circuit, this influence is proposed modeled as a varying conductance. A model for this conductance is found from an article [14] combining two classical models for electric discharge. This model is shown in eq. (3.34),

$$G_1 = G_{min} + [1 - \exp(-\frac{i_{G1}^2}{I_0^2})]\frac{U_{X7} i_{G1}}{E_0^2} + [\exp(-\frac{i_{G1}^2}{I_0^2})]\frac{i_{G1}^2}{P_0} - \theta\frac{dG_1}{dt} \tag{3.34}$$

where

$$\theta = \theta_0 + \theta_1 \exp(-\alpha|i|) \tag{3.35}$$

and the parameters in this model are shown in table 3.6.

| | Comment | | |
|---|---|---|---|
| $G_{min}$ | Least possible conductance | | |
| $\theta$ | Streamer dampening factor | | |
| $I_o$ | Limit between large and small current | | |
| $E_0$ | Constant, steady state streamer voltage | | |
| $P_0$ | Constant power loss from streamer | | |
| $i_{G1}$ | Current flowing in streamer | | |
| $U_{X7}$ | Voltage over streamer | | |

**Table 3.6:** Parameters for model for $G_1$

$G_{min}$ is the least possible conductance from the top load $C_2$ to ground. This conductance is present before any streamers form as well as after streamers have formed.

Figure 3.13 shows a streamer discharge, fig. 3.14 shows a corona discharge.

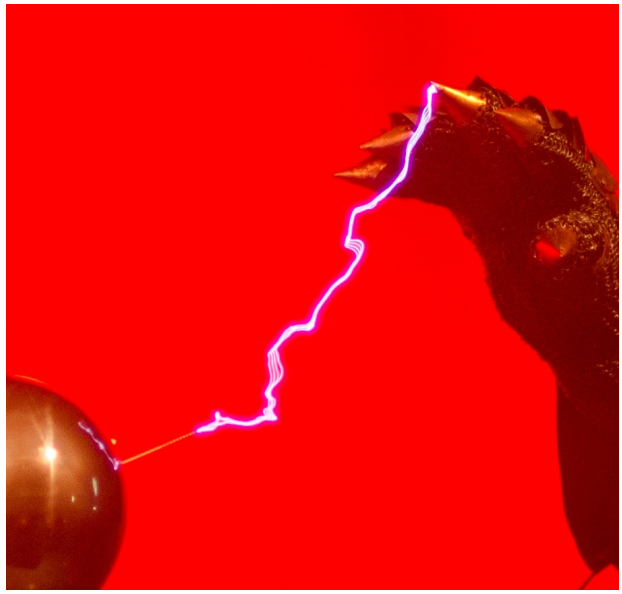

**Figure 3.13:** Streamer discharge to a grounded object
Photo: Sindre Vaskinn Hunn

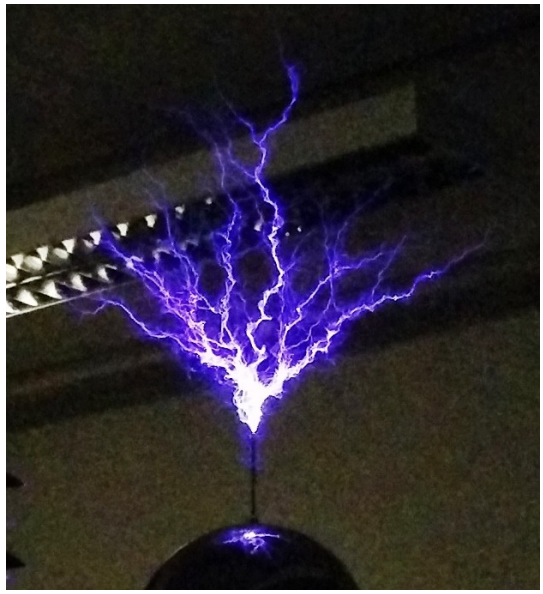

**Figure 3.14:** Corona discharge

### 3.4.1 Streamer capacitance

It is also proposed, based on the general consensus in the hobby community [15], that the streamer increases the capacitance of the top load $C_2$.

$$C_2' = C_2 + C_s = C_2 + lC_u \tag{3.36}$$

Where $C_s$ is the capacitance introduced by the streamer. $l$ is the length of the streamer in meters, $C_u$ is the capacitance of the streamer per meter. This is an approximation, the actual capacitance of the streamer can be calculated from the definition of capacitance and becomes a complicated equation that also depends on the ratio between length and width of the streamer. Two values for the capacitance per meter used in the hobby community are 25pF [4], and 5pF [12].

## 3.5 Varying parameters

Figure 3.15 shows the bode plot of the transfer function for the resonant circuit $H(s)$ with 5 different values for $R_1$, $0\Omega$, $1\Omega$, $5\Omega$, $10\Omega$, and $100\Omega$. The other parameters are given in table 3.1 for this entire section.

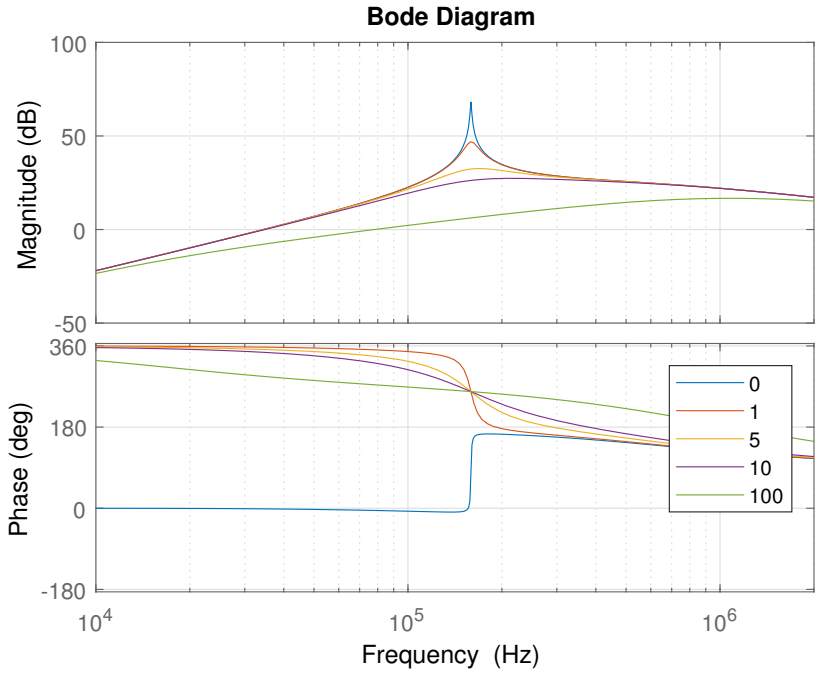


**Figure 3.15:** Bode plot of $H(s)$ varying $R_1$

Here we see that a lower resistance $R_1$ gives a sharper peak, and higher magnitude on the output.

Figure 3.16 shows the bode plot of the transfer function for the current in the primary resonant circuit $H_{FB}(s)$ with 5 different values for $R_1$, 0Ω, 1Ω, 5Ω, 10Ω, and 100Ω.

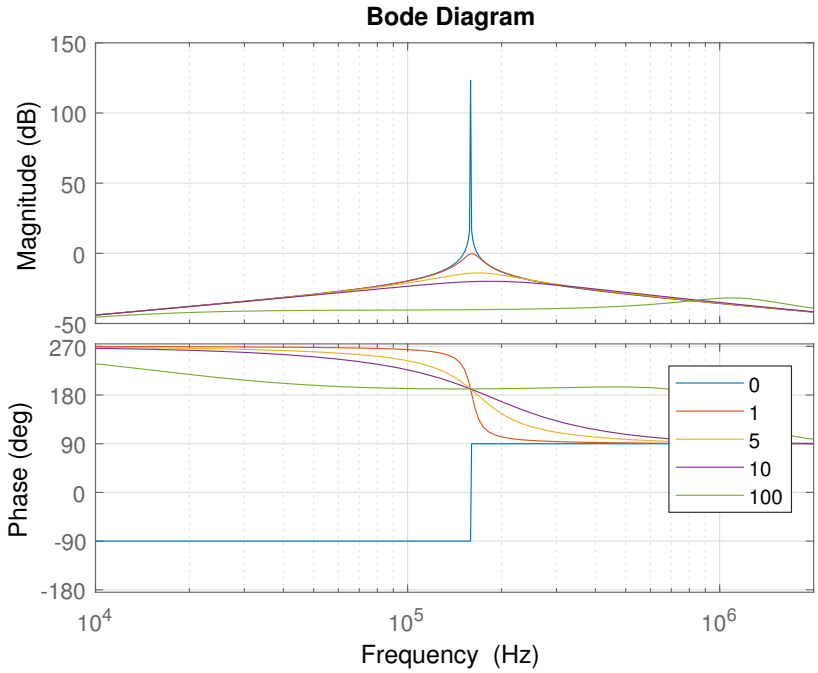


**Figure 3.16:** Bode plot of $H_{FB}(s)$ varying $R_1$

Here we see the same trend as in fig. 3.15, a lower resistance $R_1$ gives a sharper peak, and higher magnitude on the output. From this we can conclude that $R_1$ should be as low as possible. This is consistent with design recommendations in the hobby community, and the known formula for Q value eq. (3.21) for a single series resonant circuit.

Figure 3.17 shows the bode plot of the transfer function for the resonant circuit $H(s)$ with 5 different values for $R_2$, $0\Omega$, $1k\Omega$, $10k\Omega$, $100k\Omega$, and $1M\Omega$.

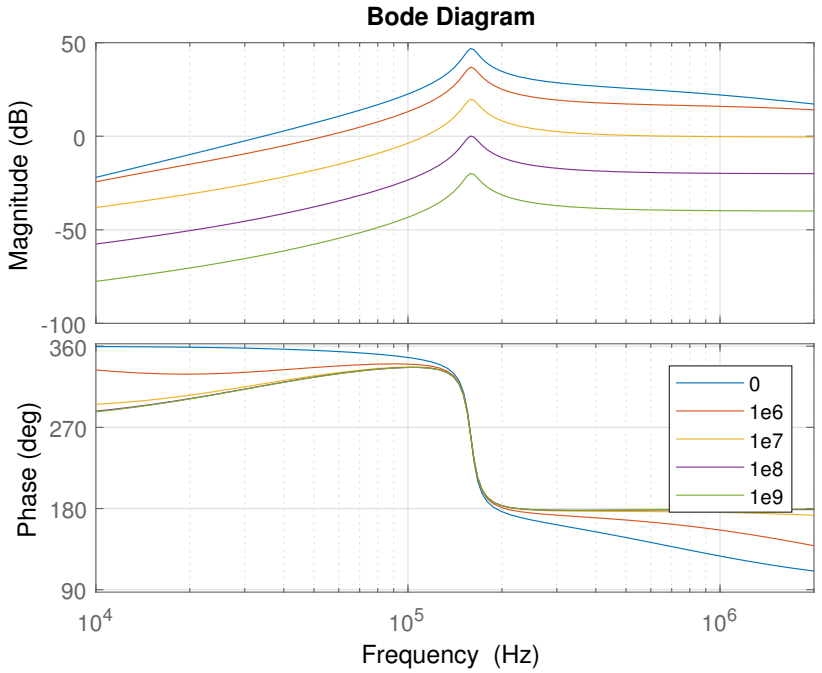


**Figure 3.17:** Bode plot of $H(s)$ varying $R_2$

Here we see that a lower resistance $R_2$ gives a higher magnitude on the output, but does not affect the sharpness of the peak.

Figure 3.18 shows the bode plot of the transfer function for the current in the primary resonant circuit $H_{FB}(s)$ with 5 different values for $R_2$, $0\Omega$, $1\Omega$, $10\Omega$, $100\Omega$, and $1k\Omega$.

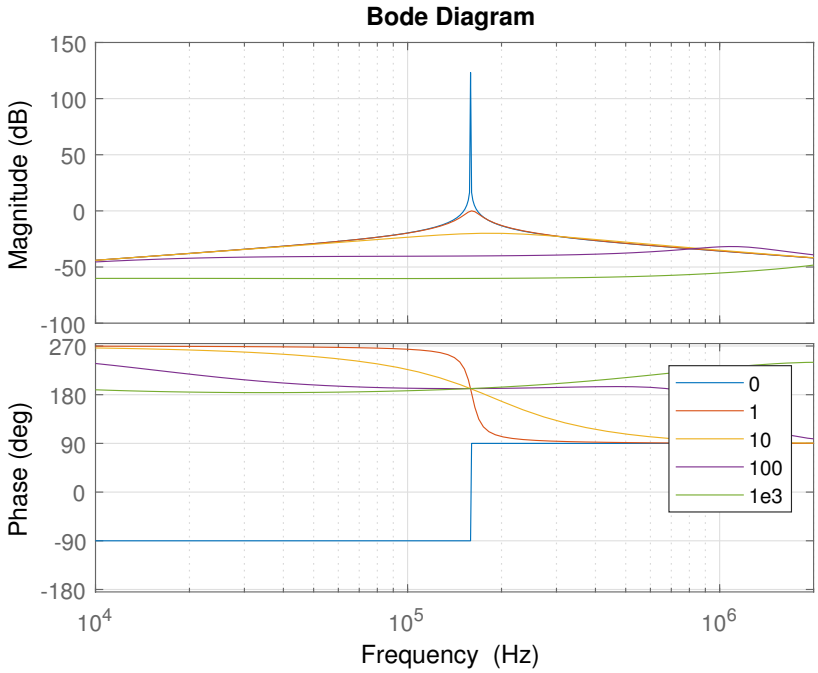


**Figure 3.18:** Bode plot of $H_{FB}(s)$ varying $R_2$

Here we see that a lower resistance $R_2$ gives a higher magnitude, and a sharper peak. From this we can conclude that $R_2$ should be as low as possible. This is consistent with design recommendations in the hobby community, and the known formula for Q value eq. (3.21) for a single series resonant circuit.

Figure 3.19 shows the bode plot of the transfer function for the resonant circuit $H(s)$ with 5 different values for $G_1$, $1T\Omega^{-1}$, $1k\Omega^{-1}$, $1\mu\Omega^{-1}$, $1p\Omega^{-1}$, and $0\Omega^{-1}$.

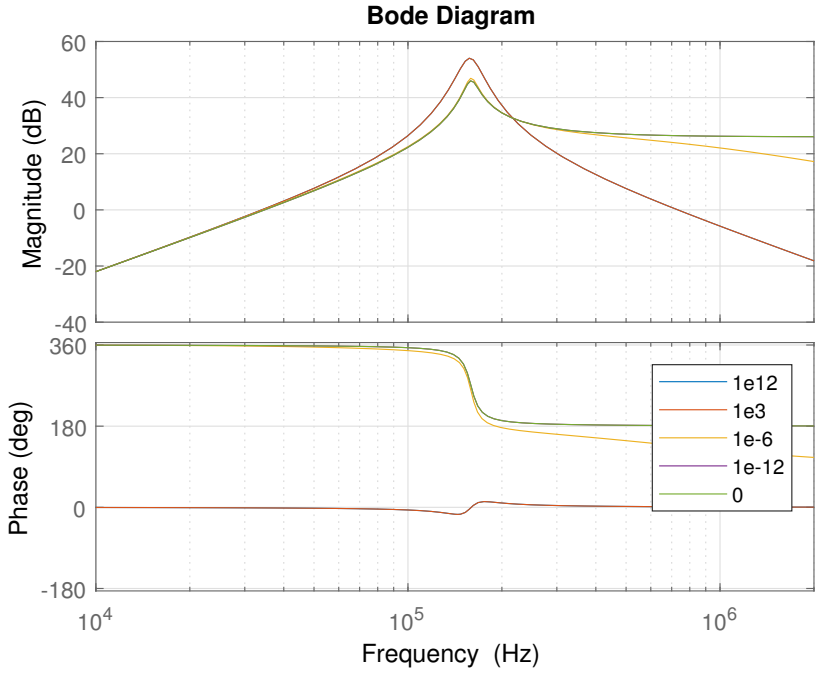


**Figure 3.19:** Bode plot of $H(s)$ varying $G_1$

Here we see that although we have a large range of values for $G_1$ the plots group in two, and there only seems to be a difference if $G_1$ is larger or smaller than 1. The top group of plots are a result of values larger than 1, and the lower group are a result of values smaller than 1. We cannot draw any significant conclusions from this.

Figure 3.20 shows the bode plot of the transfer function for the current in the primary resonant circuit $H_{FB}(s)$ with 5 different values for $G_1$, $1m\Omega^{-1}$, $100\mu\Omega^{-1}$, $10\mu\Omega^{-1}$, $1\mu\Omega^{-1}$, and $0\Omega^{-1}$.

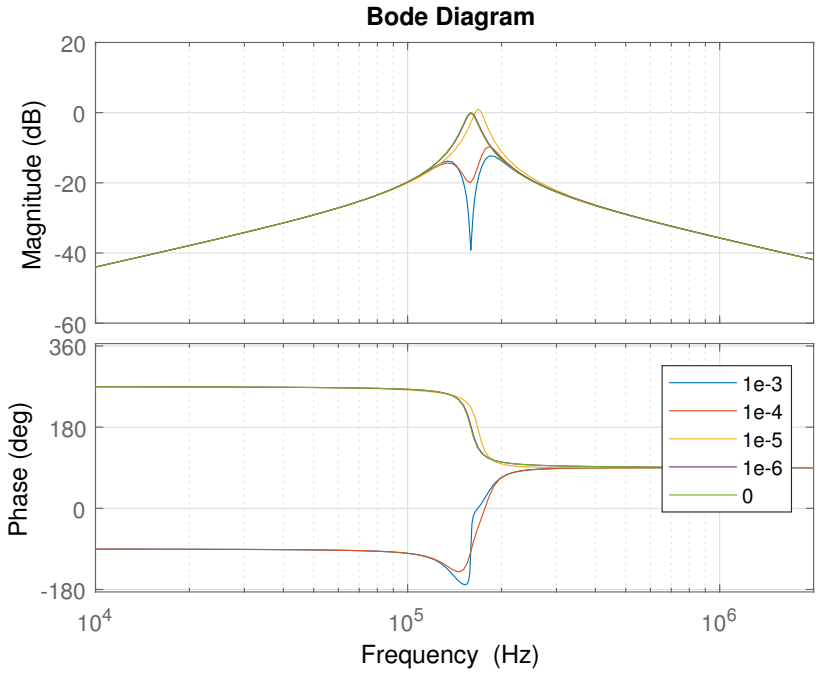


**Figure 3.20:** Bode plot of $H_{FB}(s)$ varying $G_1$

Here we see that when $G_1$ becomes larger than $1 \cdot 10^{-5}\Omega^{-1}$ we get a dip where the resonance peak was. This indicates we are unable to get any feedback signal. Thus $G_1$ should be smaller than $1 \cdot 10^{-5}\Omega^{-1}$, this is hard to control. This also implies that a streamer from the top load will affect the feedback signal, and with a too big streamer load the system with primary current feedback will be unable to function.

Figure 3.21 shows the bode plot of the transfer function for the resonant circuit $H(s)$ with 5 different values for $k$, 1.0, 0.5, 0.2, 0.1, and 0.001.

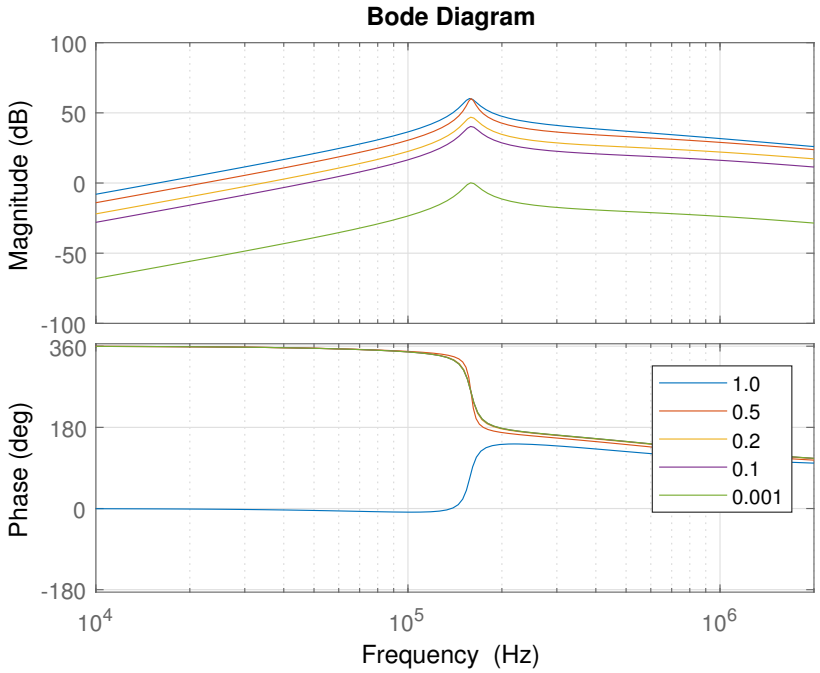


**Figure 3.21:** Bode plot of $H(s)$ varying $k$

From this we see that the closer $k$ is to 1, the larger the magnitude, the sharpness and location of the peak does not seem to be affected.

Figure 3.22 shows the bode plot of the transfer function for the current in the primary resonant circuit $H_{FB}(s)$ with 5 different values for $k$, 1.0, 0.5, 0.2, 0.1, and 0.001.

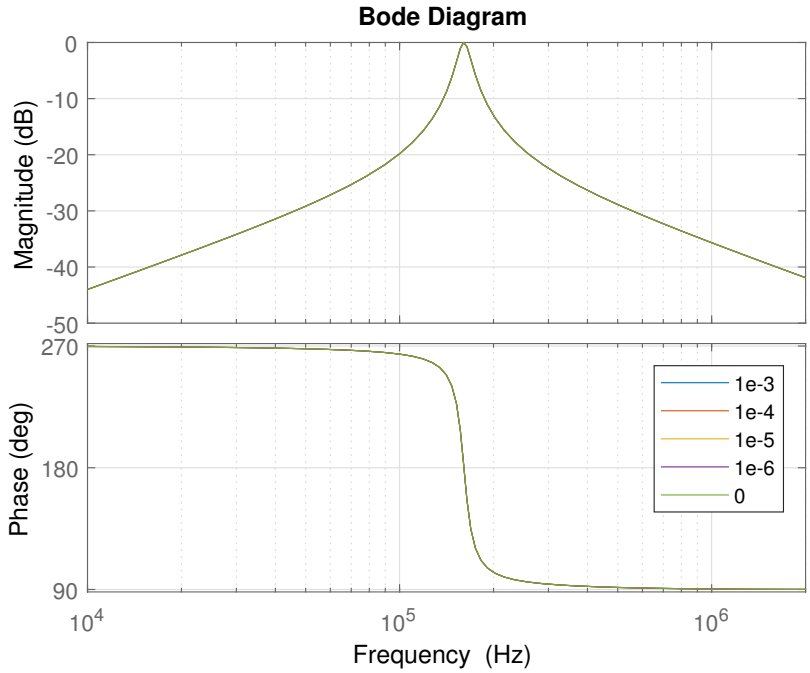


**Figure 3.22:** Bode plot of $H_{FB}(s)$ varying $k$

Here we see no effect of varying $k$. From this it may seem that a $k$ of 1 is the best. But we know from the hobby community that a $k$ above to 0.2 causes significant risk of arcing between the primary and secondary coils [12] [6] [4] [11] [5] [9].

Figure 3.23 shows the bode plot of the transfer function for the resonant circuit $H(s)$ with 5 different values for $C_1$, $0.1C_1$, $0.8C_1$, $1.0C_1$, $1.2C_1$, $10C_1$. Where $C_1 = 100$nF.

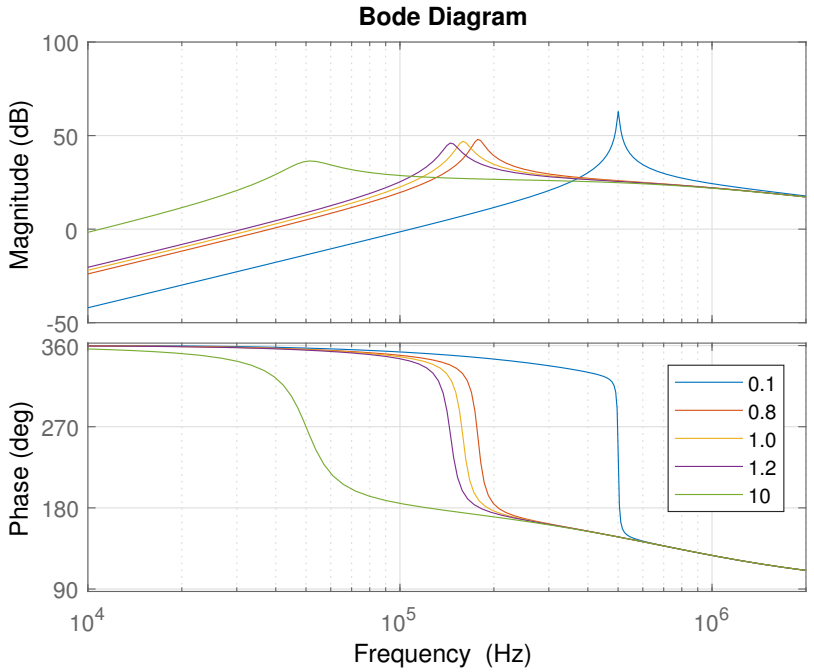


**Figure 3.23:** Bode plot of $H(s)$ varying $C_1$

From this we see that the resonance peak changes according to the change in $C_1$ as expected from the formula for resonance in a single resonance circuit. The magnitude seems to be a function of the resonance frequency, and it seems a larger magnitude may be obtained by reducing the value of $C_1$. This does not match with the hobby community recommendation of the two resonance frequencies needing to be the same.

Figure 3.24 shows the bode plot of the transfer function for the current in the primary resonant circuit $H_{FB}(s)$ with 5 different values for $C_1$, $0.1C_1$, $0.8C_1$, $1.0C_1$, $1.2C_1$, $10C_1$. Where $C_1 = 100$nF.

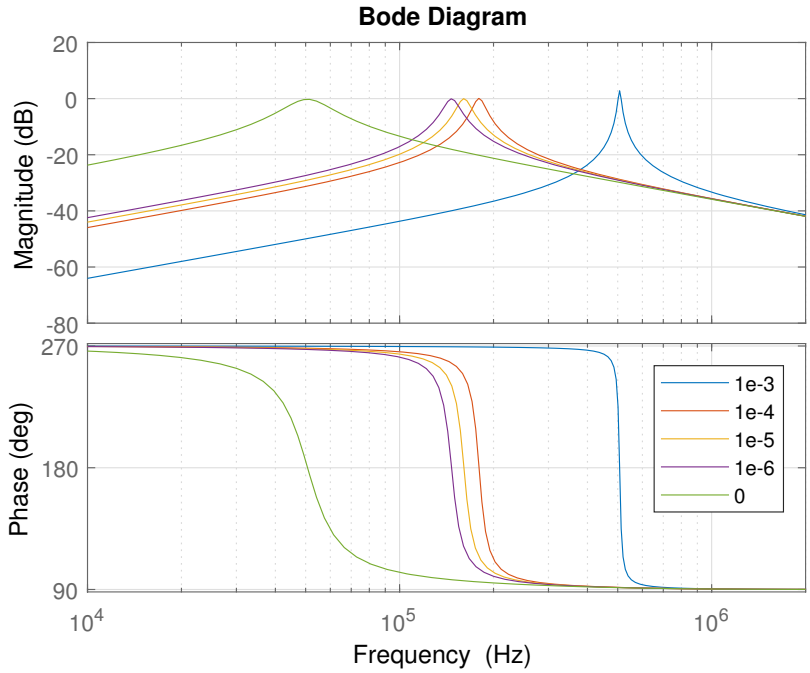


**Figure 3.24:** Bode plot of $H_{FB}(s)$ varying $C_1$

From this we see that the resonance peak changes according to the change in $C_1$ as expected from the formula for resonance in a single resonance circuit. The magnitude seems to stay the same.

Figure 3.25 shows the bode plot of the transfer function for the resonant circuit $H(s)$ with 5 different values for $C_2$; $0.01C_2$, $0.1C_2$, $1.0C_2$, $10C_2$, $100C_2$. Where $C_2 = 10\text{pF}$.

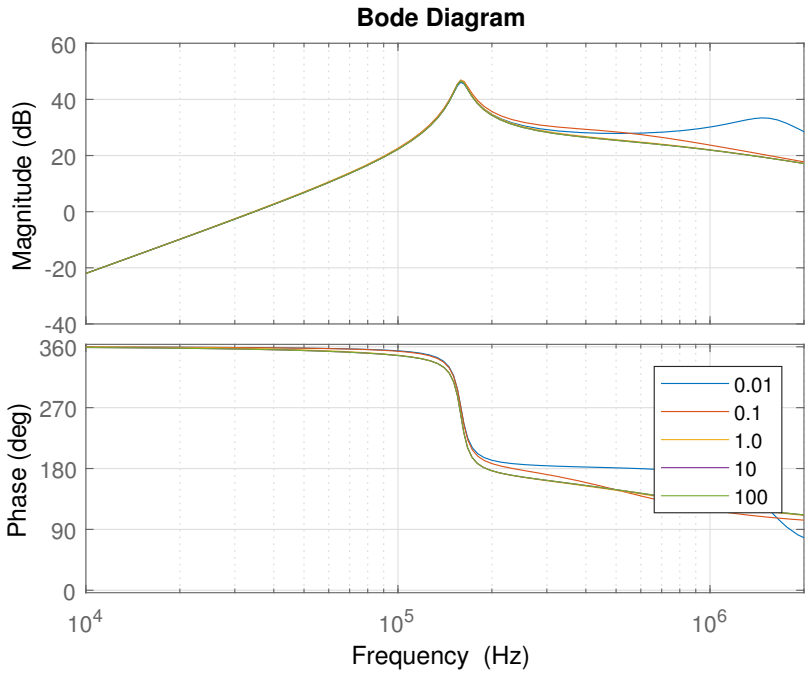


**Figure 3.25:** Bode plot of $H(s)$ varying $C_2$

Here we see very little change when varying $C_2$, we see a new peak forming when reducing $C_2$ to $0.001C_2$.

Figure 3.26 shows the bode plot of the transfer function for the current in the primary resonant circuit $H_{FB}(s)$ with 5 different values for $C_2$; $0.01C_2$, $0.1C_2$, $1.0C_2$, $10C_2$, $100C_2$. Where $C_2 = 10\text{pF}$.

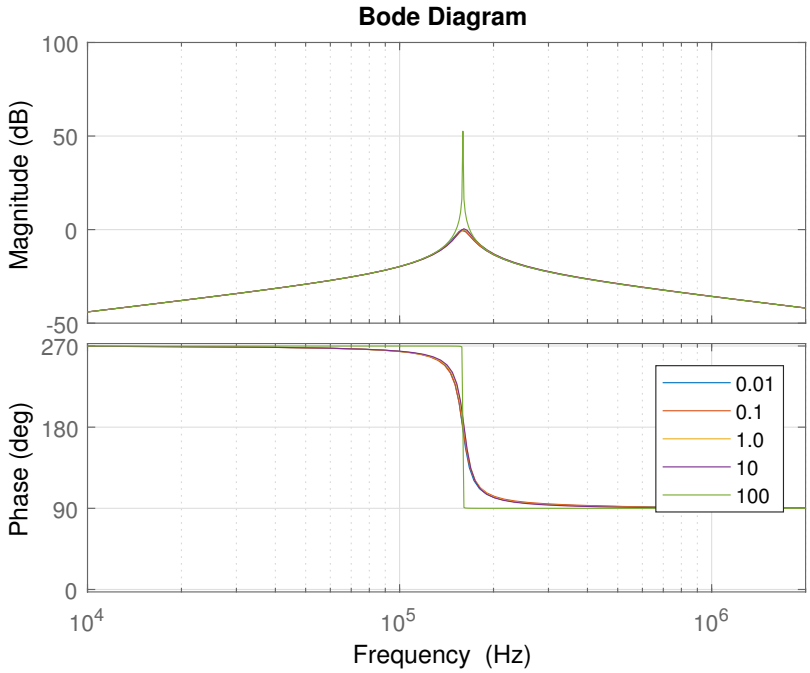


**Figure 3.26:** Bode plot of $H_{FB}(s)$ varying $C_2$

Here we see very little change when varying $C_2$. It may seem that varying $C_2$ has little effect. This does not match with the hobby community recommendation of the two resonance frequencies needing to be the same.

Figure 3.27 shows the bode plot of the transfer function for the resonant circuit $H(s)$ with 5 different values for $L_1$; $0.1L_1$, $0.8L_1$, $1.0L_1$, $1.2L_1$, $10L_1$, where $L_1 = 1 \cdot 10^{-5}$H.

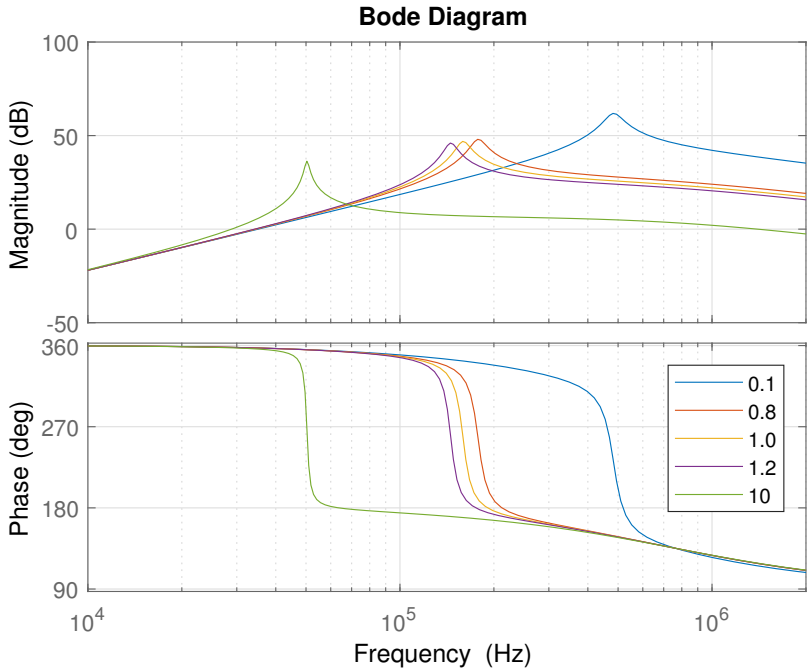


**Figure 3.27:** Bode plot of $H(s)$ varying $L_1$

From this we see that the resonance peak changes according to the change in $L_1$ as expected from the formula for resonance in a single resonance circuit. The magnitude seems to be a function of the resonance frequency, and it seems a larger magnitude may be obtained by reducing the value of $L_1$. This does not match with the hobby community recommendation of the two resonance frequencies needing to be the same.

Figure 3.28 shows the bode plot of the transfer function for the current in the primary resonant circuit $H_{FB}(s)$ with 5 different values for $L_1$; $0.1L_1$, $0.8L_1$, $1.0L_1$, $1.2L_1$, $10L_1$, where $L_1 = 1 \cdot 10^{-5}$H.

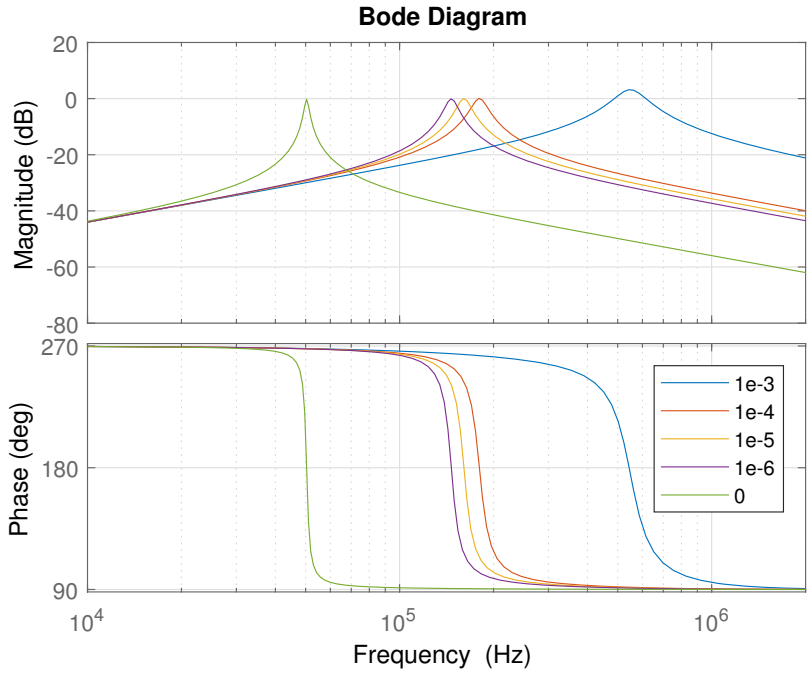


**Figure 3.28:** Bode plot of $H_{FB}(s)$ varying $L_1$

From this we see that the resonance peak changes according to the change in $L_1$ as expected from the formula for resonance in a single resonance circuit. The magnitude seems to stay the same.

Figure 3.29 shows the bode plot of the transfer function for the resonant circuit $H(s)$ with 5 different values for $L_2$; $0.01L_2$, $0.8L_2$, $1.0L_2$, $1.2L_2$, $100L_2$, where $L_2 = 1 \cdot 10^{-1}$H.

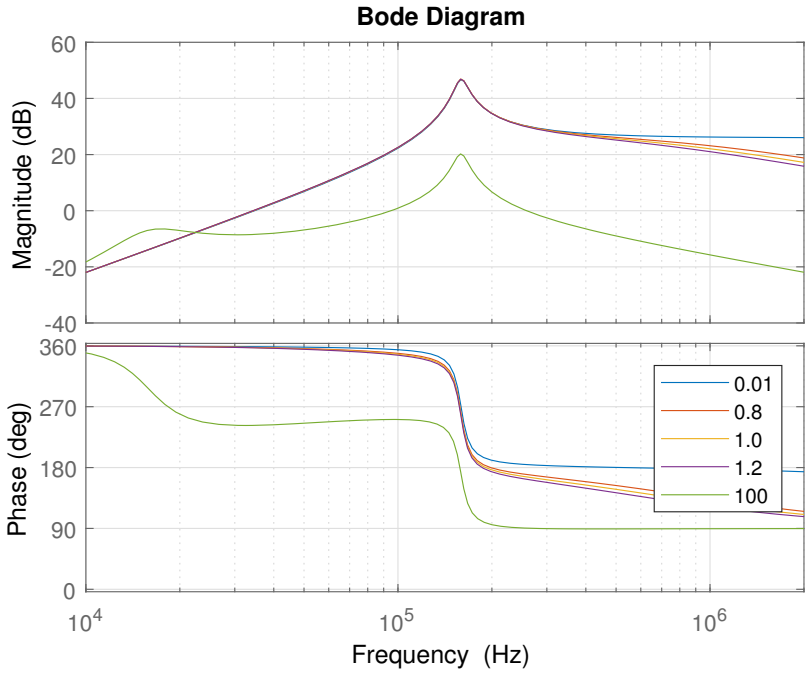


**Figure 3.29:** Bode plot of $H(s)$ varying $L_2$

Here we see little in resonance peak location or magnitude, apart from $100L_2$ where the magnitude is drastically reduced.

Figure 3.30 shows the bode plot of the transfer function for the current in the primary resonant circuit $H_{FB}(s)$ with 5 different values for $L_2$; $0.01L_2$, $0.8L_2$, $1.0L_2$, $1.2L_2$, $100L_2$, where $L_2 = 1 \cdot 10^{-1}$H.

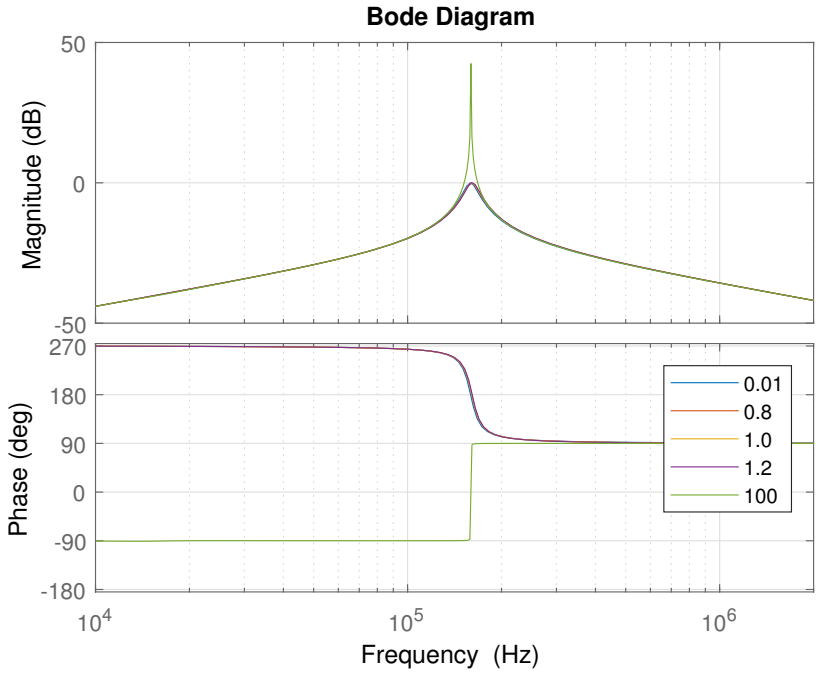


**Figure 3.30:** Bode plot of $H_{FB}(s)$ varying $L_2$

Here we see little in resonance peak location or magnitude, apart from $100L_2$ where the magnitude is drastically increased. It may seem that varying $L_2$ has little effect. This does not match with the hobby community recommendation of the two resonance frequencies needing to be the same.

# Chapter 4

# Measurements

To confirm that the signals $X1$-$X9$ have the alleged behaviour measurements have been done on a physically implemented DRSSTC, with the component values shown in the schematics in this thesis. The DRSSTC the measurements are done on is the one constructed by Omega Verksted [20] [21].

## 4.1 Voltage measurements

The voltage measurements of the tesla coil were performed in the high voltage laboratory at the department of electrical power engineering at NTNU.

Figure 4.1 shows the signal $X1$ into the pulse shaper and the resulting signal $X2$ on the output of the pulse shaper. The interrupter and power amplifier is not connected.

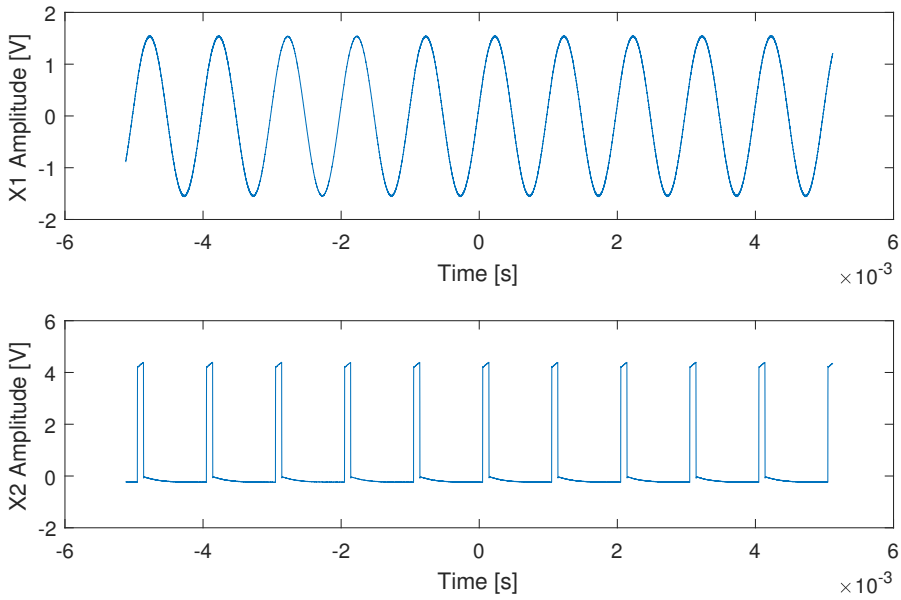


**Figure 4.1:** $X1$X2

Here we see that the sinusoidal signal $X1$ with zero DC component is transformed into a two level signal $X2$ between 0V and 5V. We also see that it has a constant duty cycle.

Figure 4.2 shows the same signals $X1$ and $X2$ as in fig. 4.1 but also shows the output of the interrupter $X4$ as well as the feedback signal $X8$. Note that $X2$ is measured after the optical channel (section 2.8).

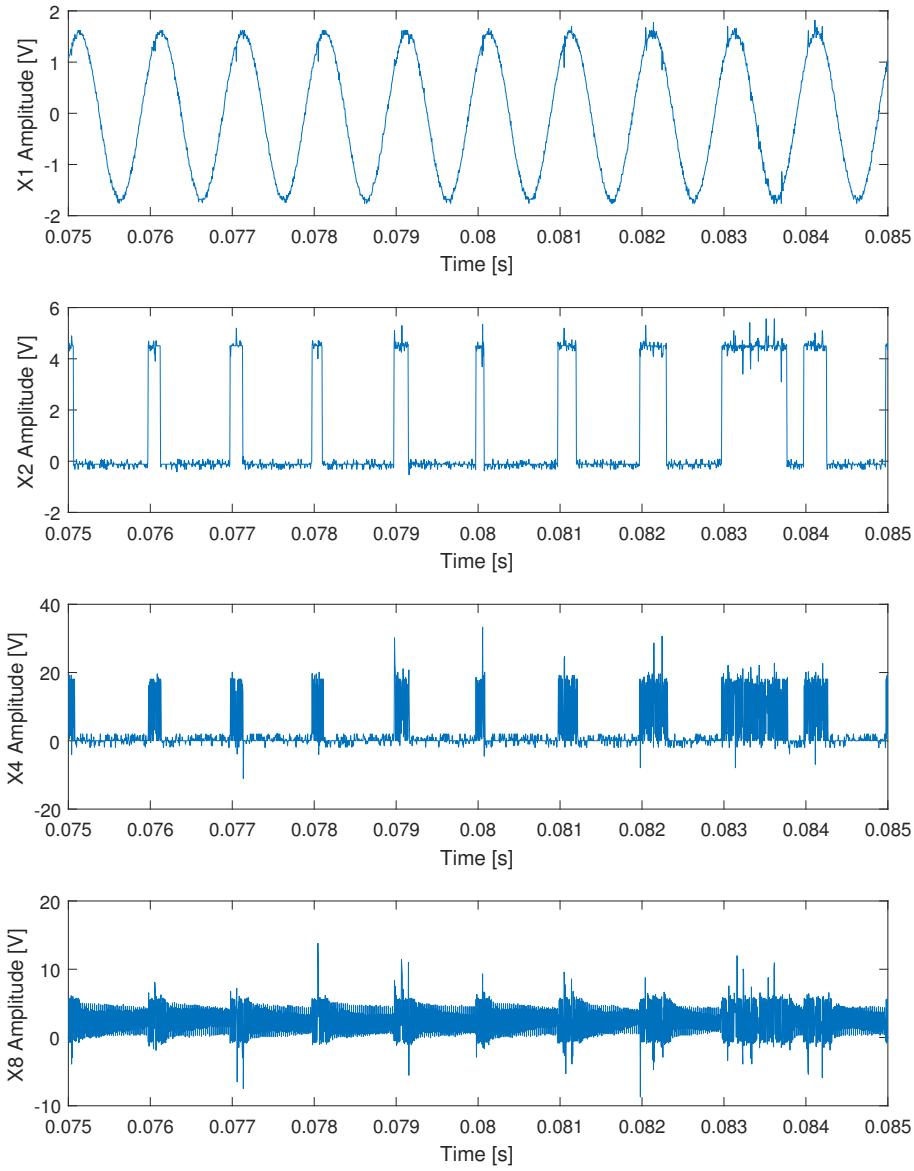


**Figure 4.2:** $X1\ X2\ X4\ X8$

First it is worth noting that we have more noise in fig. 4.2 than in fig. 4.1 because the interrupter, power amplifier, and resonant circuit are connected and turned on. We see that this electromagnetic noise affects how well $X2$ is generated, and the duty cycle is no longer constant. This is a source of noise on the output acoustic signal. The envelope of $X4$ follows $X2$ as expected. The envelope of $X8$ follows $X2$ as well as it having a ring down.

Figure 4.3 shows the voltage on the output of the power amplifier $U_{X6}$.

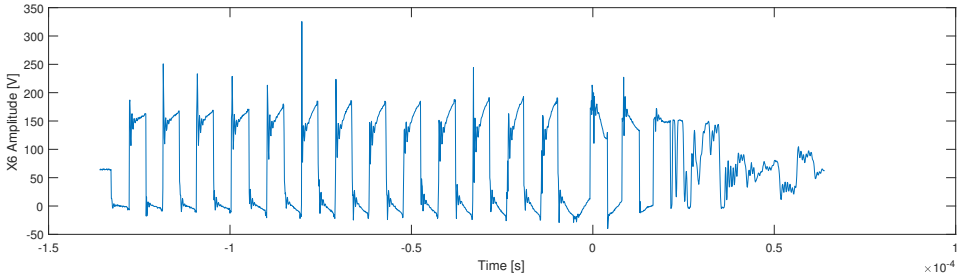


**Figure 4.3:** $X6$

Here we see a positive square wave with 50% duty cycle and amplitude from 0V to 160V, and a duration of 13 cycles before being turned off. After this wave train we see the ring down of the voltage on the resonant circuit.

## 4.2 Acoustic measurements

The acoustic measurements of the tesla coil were performed in the high voltage laboratory at the department of electrical power engineering at NTNU. This was the only location fitting after health and safety considerations were made. This room is not designed for acoustic measurements, and has significant ambient noise and reflections.

The coil rig were placed in the room with a grounding electrode consisting an orb and spike with identical design as the topload placed a distance of 40cm away. The driver was placed 3 meters away connected with a 3m long cable. The signal generator, pulse shaper, and recording equipment was placed adjacent to the driver.

The recording was performed by the department of acoustics at ntnu.

Since the room was not meant for acoustic measurements the impulse response of the room was measured. This measurement was also performed by the department of acoustics at ntnu. This was done by placing a speaker approximately in the center of the room, and a microphone were the microphone was to be placed during recordings. Then a sweep was played on the speaker, and recorded.

The recordings of single tones was performed by setting the signal generator to the wanted input frequency and then the output sound was recorded.

The recordings of musical audio files was performed by playing the file from a computer and then recording the output sound.

The sweep was recorded by playing a sweep from a different computer, and then recording, When playing the sweep we discovered that the computer playing back the sweep (and recording) was affected by the electromagnetic field generated by the tesla coil, and the playback was thus choppy. It was later discovered that all recordings done were choppy.

The acoustic measurements done but not discussed here is attached in appendix B

Figure 4.4 shows a periodogram of the recorded audio signal with a 1kHz input on $X2$. The amplitude is the energy of the signal and the x-axis shows the frequency.

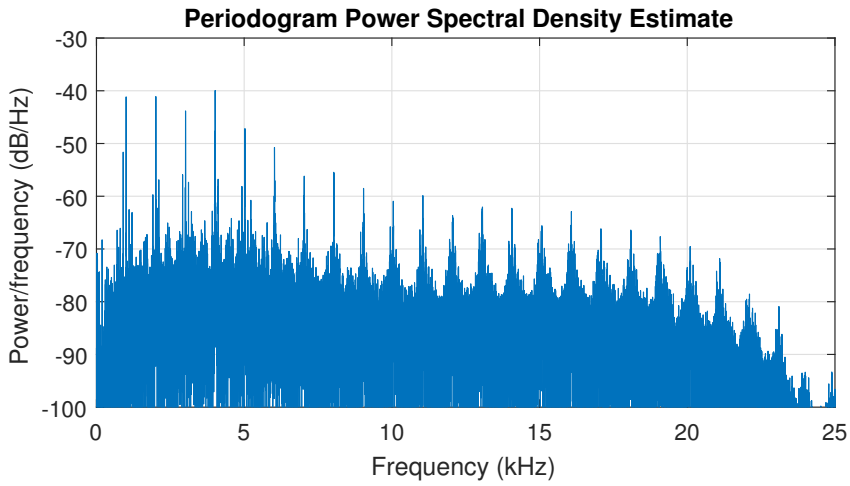


**Figure 4.4:** Periodogram of 1kHz recorded tone

Here we see the base frequency 1kHz and harmonics spaced 1kHz apart all the way through the range of human hearing. We see that the lowest three harmonics together with the base frequency are dominant, then the energy of the harmonics start to decrease. This implies the waveform rises sharply and has a short duration, which is consistent with a series of electrical discharges. The amplitudes of the harmonics are shown in table 4.1.

Figure 4.5 shows the waveform of the recorded audio signal with a 1kHz input on $X2$.

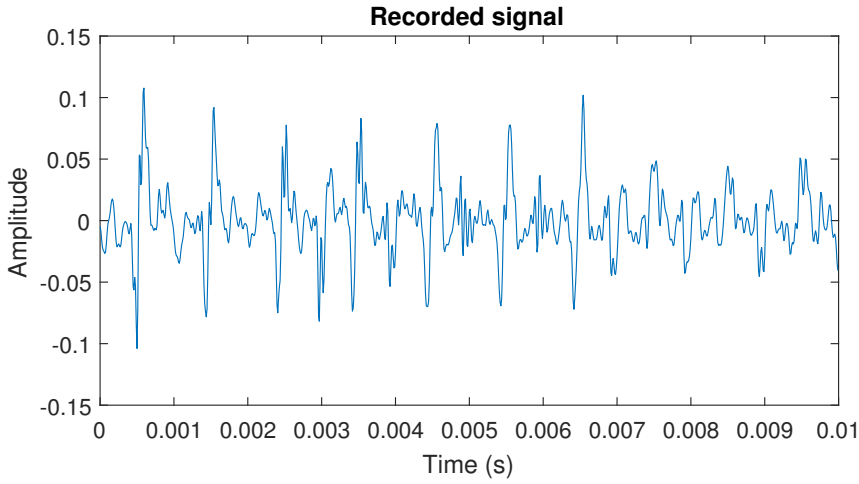


**Figure 4.5:** Time domain plot of 1kHz recorded tone

Here we see a dominant series of pulses with frequency 1kHz, we also see that it has several higher harmonics. Which is consistent with fig. 4.4. The signal also appears to be noisy.

Figure 4.6 shows the recorded signal compared to a signal generated in matlab with the amplitudes read from the periodogram of the recorded signal and shown in table 4.1.

| Frequency (Hz) | Amplitude (dB/Hz) |
|---|---|
| 1k | -41 |
| 2k | -41 |
| 3k | -44 |
| 4k | -40 |
| 5k | -47 |
| 6k | -51 |
| 7k | -55 |
| 8k | -55 |
| 9k | -58 |
| 10k | -60 |
| 11k | -60 |
| 12k | -64 |
| 13k | -62 |
| 14k | -62 |
| 15k | -65 |
| 16k | -62 |
| 17k | -66 |
| 18k | -66 |
| 19k | -67 |
| 20k | -70 |
| 21k | -72 |
| 22k | -80 |

**Table 4.1:** Amplitudes of the harmonics

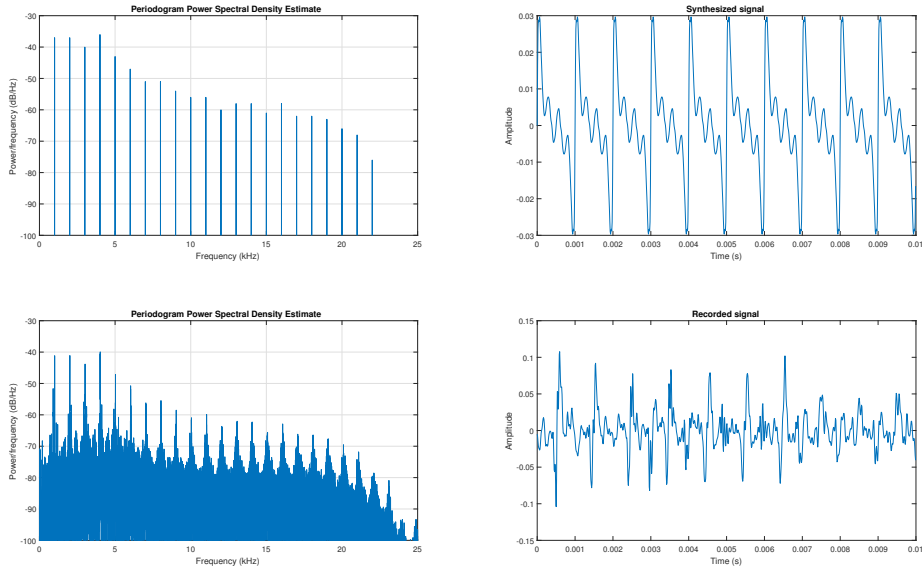


**Figure 4.6:** Comparison of recorded tone and synthesized tone

From this figure we see that the reconstructed signal matches well with the exception of the reconstructed signal not having any frequency components other than the harmonics.

# Chapter 5

# Conclusion

An implementation of a DRSSTC has been analyzed and described. The intended function of components have been presented and substantiated with mathematics. The component values or parameters that need to be adapted to the resonant frequency are; the delay in the latch reset network $t_r$ given by $R_3$ and $C_2$ in the interrupter, the phase lead time $t_d$ given by $L_1$ and $R_2$ in the interrupter, and the corner frequency of the noise filter $f_c$ given by $R_2$ and $C_3$ in the limiter. $t_r$ affects the acoustic signal if the synchronous shutdown in the interrupter does not function correctly. $t_d$ affects the heat generated in the power amplifier, and the amplitude on the output. $f_c$ can affect noise on the acoustic signal.

The component values or parameters that need to be adapted to the current flowing in the primary resonant circuit $I_1$ are; $|Z_L|$ given by $L_1$ and $R_2$ in the interrupter, $R_2$ in the limiter, and the number of turns $n$ on $L_3$ and $L_4$ in the primary resonant circuit. $|Z_L|$ affects. $R_2$ affects the range of amplitude attainable on the output. $n$ affects the selection of $|Z_L|$ and $R_2$.

In the resonant circuit we have shown that the ohmic resistances $R_1$ and $R_2$ in both the primary and secondary circuit should be as small as possible to give a high as possible amplitude on the output, the conductance of the streamer $G_1$ does not seem to affect the resonant frequency (detuning) or the amplitude on the output, but does affect the current in the primary resonant circuit. And will affect the feedback signals $X8$ and $X9$. The coupling coefficient $k$ only affects the amplitude on the output, as long as no arcing happens between the primary and secondary coils $L_1$ and $L_2$. According to the transfer functions $H(s)$ and $H_{FB}(s)$ varying $C_1$, $L_1$, $C_2$, or $L_2$ does not give the same results as expected from the common assumptions in the hobby community. Here no other conclusions can be drawn other that this may

be a topic for further research.

The electrical measurements done on the physical implementation further substantiate the mode of operation of the driver. The acoustic measurements substantiate that an acoustic signal can be generated with the circuits presented here, and may be used for further research on the streamer and any alternative or related ways of generating an acoustic signal with a tesla coil. This report may also give an operator insight into what input signals $X1$ are suitable for this implementation of driver.

## 5.1 Topics for further research

There is a broad agreement in the hobby community that the streamer affects the system, but its effects on the system are not clear from the work done here. Parameters for the streamer model mentioned should be found to further investigate how the streamer influences the voltages and currents on the output.

The component values and parameters and its effect on the output signal are only substantiated with theoretical work and should be verified experimentally.

By varying the supply voltage for the power amplifier one could acheive AM modulation instead of PDM modulation.

When pulses on the input $X2$ get too close, the coil rig has not had time to swing down, if a new pulse is input before it has swung down one may risk switching while the current is not zero, and the response may be different. It would be interesting to investigate wether the latch in the interrupter will or can be used to keep the signal $X5$ in sync.

# Bibliography


[1] Chip Atkinson. Tesla coil mailing list. http://www.pupman.com/, 2016. [Online; accessed 2016-11-17].

[2] H.D. B. Radio transmission systems with modulatable passive responder, March 1 1960. US Patent 2,927,321.

[3] A. M. Cassie. Arc rupture and circuit serverity: A new theory. *CIGRE Rep.*, 102, 1939.

[4] Steve Conner. Steve conners amazing tesla coils. http://www.scopeboy.com/tesla/index.html, 2007. [Online; accessed 2017-06-23].

[5] Terry Fritz. Terry's drsstc site. http://www.drsstc.com/~terrel, 2005. [Online; accessed 2017-06-23].

[6] Gao Guangyan. Loneoceans laboratories. http://www.loneoceans.com, 2016. [Online; accessed 2017-06-23].

[7] Gao Guangyan. Universal drsstc tesla coil driver 2.7 rev c. http://www.loneoceans.com/labs/ud27/, 2016. [Online; accessed 2017-06-23].

[8] S. L. Ho, J. Wang, W. N. Fu, and M. Sun. A comparative study between novel witricity and traditional inductive magnetic coupling in wireless charging. *IEEE Transactions on Magnetics*, 47(5):1522–1525, May 2011.

[9] Jimmy Hynes. Drsstc.com. http://www.drsstc.com/, 2005. [Online; accessed 2017-06-23].

[10] O. Mayr. Beitrage zur theorie des statischen und des dynamischen lichbogens. *Archiv fur Elektrotechnik*, 37:588–608, 1943.

[11] Dan McCauley. Eastern voltage research. http://www.easternvoltageresearch.com/, 2013. [Online; accessed 2017-06-23].

[12] Terry. Scantesla. http://www.pupman.com/listarchives/2006/Jun/msg00083.html, 2006. [Online; accessed 2017-06-23].

[13] N. Tesla. Experiments with alternate currents of very high frequency and their application to methods of artificial illumination. *Transactions of the American Institute of Electrical Engineers*, VIII(1):266–319, Jan 1891.

[14] King-Jet Tseng, Yaoming Wang, and D. M. Vilathgamuwa. An experimentally verified hybrid cassie-mayr electric arc model for power electronics simulations. *IEEE Transactions on Power Electronics*, 12(3):429–436, May 1997.

[15] Uspring. A streamer load measurement with a drsstc. http://4hv.org/e107_plugins/forum/forum_viewtopic.php?137883, 2012. [Online; accessed 2017-06-28].

[16] R. Want. Near field communication. *IEEE Pervasive Computing*, 10(3):4–7, July 2011.

[17] Steve Ward. Steve's high voltage. http://www.stevehv.4hv.org/, 2008. [Online; accessed 2017-06-23].

[18] H. A. Wheeler. Simple inductance formulas for radio coils. *Proceedings of the Institute of Radio Engineers*, 16(10):1398–1400, Oct 1928.

[19] Wikipedia. Streamer discharge — wikipedia, the free encyclopedia, 2017. [Online; accessed 28-June-2017 ].

[20] Øystein Smith. Portable and reliable drsstc demonstrator. https://github.com/Cable89/TFE4520-Prosjektoppgave/, 2017. [Online; accessed 2017-06-28].

[21] Øystein Smith et. al. Tesla-driver git repository. https://github.com/Cable89/tesla-driver, 2016. [Online; accessed 2016-12-17].

# Appendix A

# Matlab code

## A.1 Transfer

```
C1 = 1e-7;
C2 = 1e-11;
L1 = 1e-5;
L2 = 1e-1;
k = 0.2;
M = k*sqrt(L1*L2); %2e-6;
R1 = 1;
R2 = 1e2;
G1 = 2e-6;

fprintf('Expected resonance frequency:\n');
fprintf('%i Hz\n', 1./(2*pi()*sqrt(C1*L1)));

H1 = trans(C1, C2, L1, L2, M, R1, R2, G1);
%H2 = trans(C1, C2, L1, L2, M, R1, R2, G1);
%H3 = trans(C1, C2, L1, L2, M, R1, R2, G1);
%H4 = trans(C1, C2, L1, L2, M, R1, R2, G1);
%H5 = trans(C1, C2, L1, L2,  M, R1, R2, G1);

figure('Name','L2');
bde1 = bodeplot(H1);%,H2,H3,H4,H5);
setoptions(bde1, 'FreqUnits','Hz','Grid','on','Xlim'
    ,[1e4, 2e6]);
%legend('0.01','0.8','1.0','1.2','100','Location','
```

```
    northeast');

[mag, phase, W] = bode(H1);
[val, idx] = max(20*log10(squeeze(mag(1,1,:))));
W = W./(2*pi);
fprintf('Max amplitude:\n');
fprintf('%i dB\n', val);
fprintf('%i Hz\n', W(idx));

figure;
subplot(2,1,1)
step(H1, 2e-5); hold on;
[Y, T] = step(H1, 2e-5);
%findpeaks(Y)
[pks1, locs1] = findpeaks(-Y);
[pks2, locs2] = findpeaks(Y);
stepfrequency = 1./(2*(T(locs2(1))-T(locs1(1))))


subplot(2,1,2)
impulse(H1, 2e-5);

figure;
pzplot(H1);
grid on;
[P, Z] = pzmap(H1)

function H = trans(C1, C2, L1, L2, M, R1, R2, G1)
    a = ((C1*C2*G1*L1*L2)-2*(C1*C2*G1*L1*M)+(C1*C2*G1
        *M^2));
    b = ((C1*C2*G1*L1*R2)+(C1*C2*G1*L2*R1)-2*(C1*C2*
        G1*M*R1)+(C1*C2*L1));
    c = ((C1*C2*G1*R1*R2)+(C1*C2*R1)+(C1*G1*L1)+(C2*
        G1*L2)-2*(C2*G1*M));
    d = ((C1*G1*R1)+(C2*G1*R2)+C2);
    e = (G1);
    f = (-1)*(C1*C2*M);
    g = (-1)*(C1*G1*M);

    H = tf([f g 0 0],[a b c d e]);
```

```
60 end
61
62 function H = transferCurrent(C1, C2, L1, L2, M, R1, R2
       , G1)
63     a   = 2*(C1*C2*G1*M)-(C1*C2*G1*L2);
64     b   = 0-(C1*C2*G1*R2)-(C1*C2);
65     c   = 0-(C1*G1);
66     d   = 0;
67     e   = (C1*C2*G1*L1*L2)-2*(C1*C2*G1*L1*M);
68     f   = (C1*C2*G1*L1*R2)+(C1*C2*L1)+(C1*C2*G1*R1*L1)
           -2*(C1*C2*G1*R1*M);
69     g   = (C1*G1*L1)+(C1*C2*R1)+(C2*G1*L2)-2*(C2*G1*M);
70     h   = (C1*G1*R1)+(C2*G1*R2)+C2;
71     k   = G1;
72
73     H   = tf([a b c d],[e f g h k]);
74 end
```

## A.2 Linear simulation

```
C1 = 1e-7;
C2 = 1e-11;
L1 = 1e-5;
L2 = 1e-1;
k = 0.2;
M = k*sqrt(L1*L2); %2e-6;
R1 = 1;
R2 = 1e2;
G1 = 2e-6;
%G1 = 2e-7;

% Time domain parameters
fs = 4e6;          % Sampling frequency
dt = 1/fs;         % Time resolution
T = 1;             % Signal duration
t = 0:dt:T-dt;     % Total duration
N = length(t);     % Number of time samples


f0=1/(2*pi*(sqrt(L1*C1)))
f0_s=1/(2*pi*(sqrt(L2*C2)))
f0=1.57e+05
T0 = (fs/f0);
n = 10;

x2=square(2*pi*f0*t);
x2 = x2*160;
x2 = x2(1:int16(n*T0));
x2 = [x2 zeros(1,(N-length(x2)), 'int16')];

H = trans(C1, C2, L1, L2, M, R1, R2, G1);

figure;

lsim(H,x2,t);
axis([0 1.5e-4 -5e4 5e4]);
xlabel('Time [s]');
ylabel('Amplitude [V]');
pbaspect([2 1 1]);
```

## A.3 Limiter filter

```
R2 = 10;
C3 = 1e9;
n1 = 1;
n2 = 100;

H = tf([R2],[R2*C3 1])

bodeplot(H);
[mag,phase,wout] = bode(H);
```

## A.4 Audio plot and synthesis

```
%% Time domain parameters
fs = 96000;       % Sampling frequency
dt = 1/fs;        % Time resolution
T = 5;            % Signal duration
t = 0:dt:T-dt;    % Total duration
N = length(t);    % Number of time samples

%% Signal generation
envelope = [-41 -41 -44 -40 -47 -51 -55 -55 -58 -60
    -60 -64 -62 -62 -65 -62 -66 -66 -67 -70 -72 -80]; %
     In dB/Hz
envelope = db2mag(envelope);
%envelope = envelope+10;
f0 = 1000;        % fundamental frequency
x = envelope(1)*sin(2*pi*f0*t); % fundamental sinusoid
for i = 2:22
    x = x + envelope(i)*sin(2*pi*f0*i*t);
end

%% Magic
[y,fsy] = audioread('1khz - 09.wav');
y = y(fs*2:fs*7);

%% Generated
figure;
subplot(2,2,1);
plot(psd(spectrum.periodogram,x,'Fs',fs,'NFFT',length(
    x)));
axis([0 25 -100 -30]);
px = audioplayer(x, fs);
%play(px, [1 (get(px, 'SampleRate') * 3)]);
subplot(2,2,2);
plot(t(1:fs*1e-2), x(1:fs*1e-2));
title('Synthesized signal');
xlabel('Time (s)');
ylabel('Amplitude');
%pause(6);

%% Measured
```

```
37 subplot(2,2,3);
38 plot(psd(spectrum.periodogram,y,'Fs',fs,'NFFT',length(
       y)));
39 axis([0 25 -100 -30]);
40 py = audioplayer(y, fs);
41 subplot(2,2,4);
42 plot(t(1:fs*1e-2), y(1:fs*1e-2));
43 title('Recorded signal');
44 xlabel('Time (s)');
45 ylabel('Amplitude');
46 %play(py, [1 (get(py, 'SampleRate') * 3)]);
47
48 figure;
49 plot(psd(spectrum.periodogram,y,'Fs',fs,'NFFT',length(
       y)));
50 axis([0 25 -100 -30]);
51 pbaspect([2 1 1])
52 figure;
53 plot(t(1:fs*1e-2), y(1:fs*1e-2));
54 pbaspect([2 1 1]);
55 title('Recorded signal');
56 xlabel('Time (s)');
57 ylabel('Amplitude');
```

# Appendix B

# Acoustic measurements

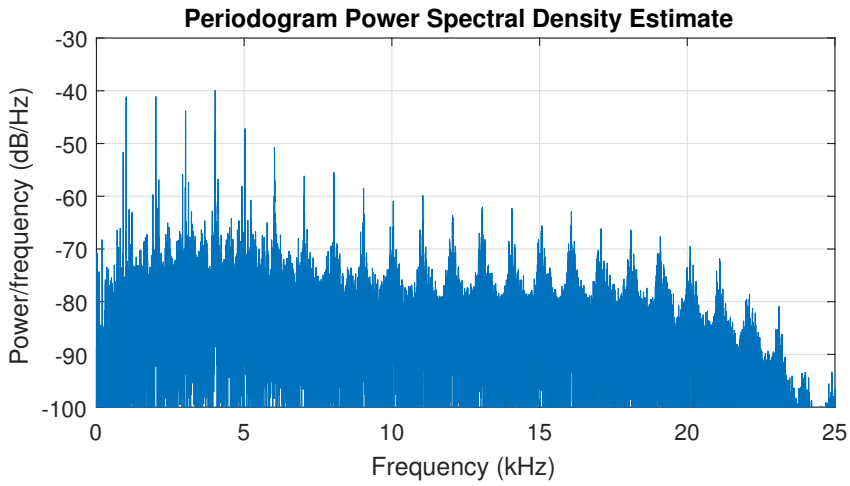


**Figure B.1:** Periodogram of 1kHz recorded tone, duty cycle 09.

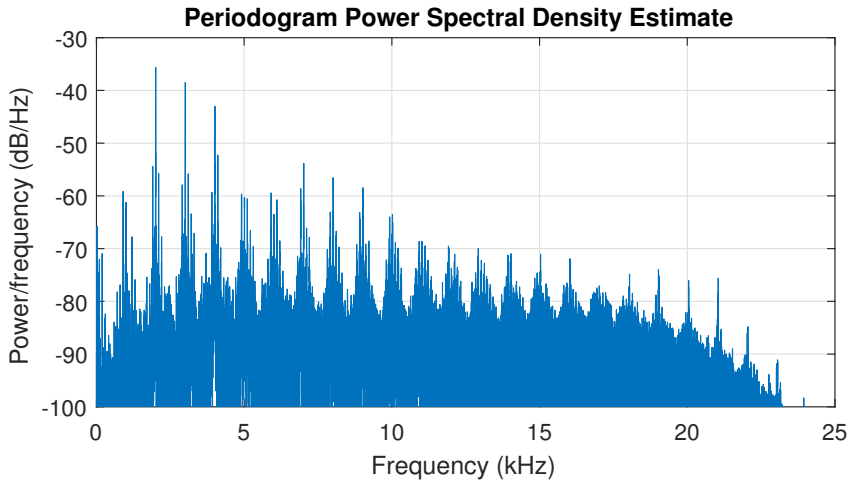


**Figure B.2:** Periodogram of 1kHz recorded tone, duty cycle 10.

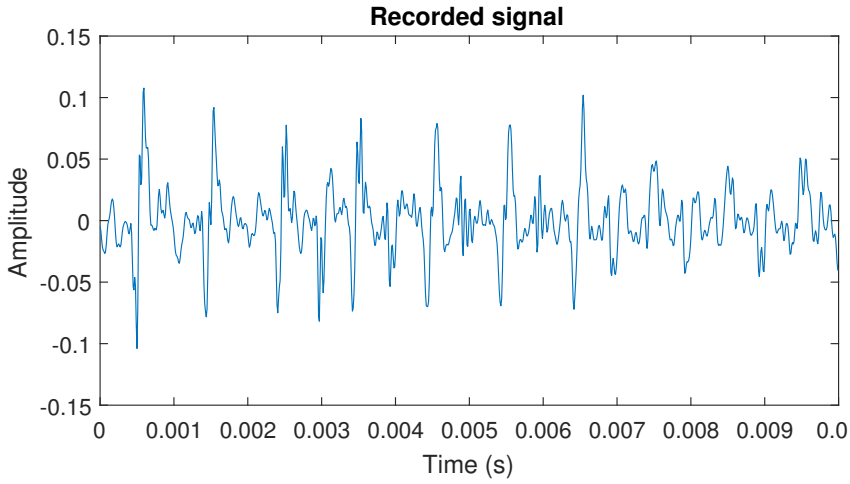


**Figure B.3:** Time domain plot of 1kHz recorded tone, duty cycle 09.

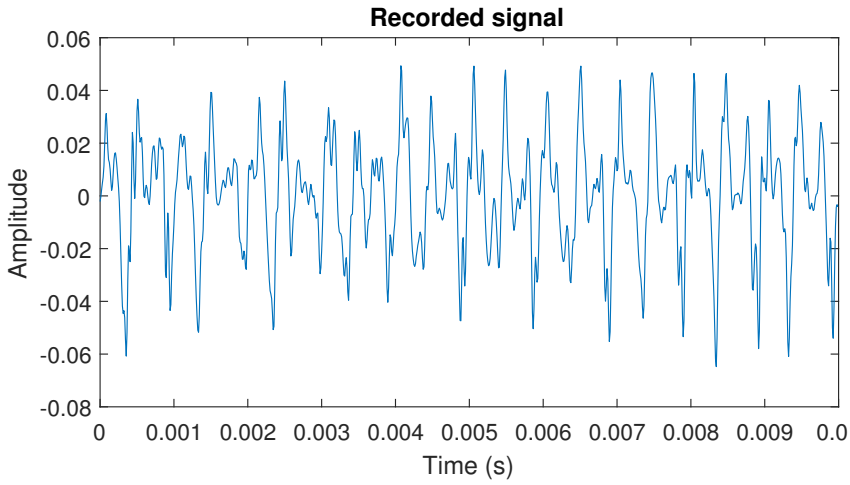


**Figure B.4:** Time domain plot of 1kHz recorded tone, duty cycle 10.

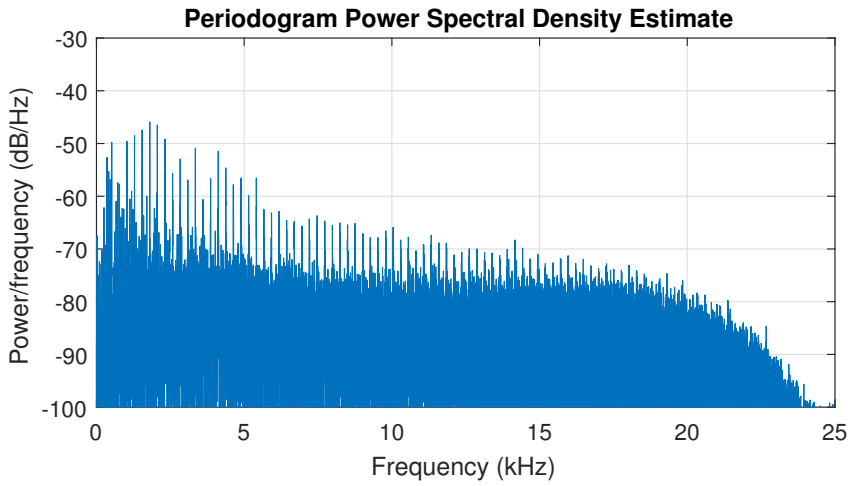


**Figure B.5:** Periodogram of 250Hz recorded tone, duty cycle 09.

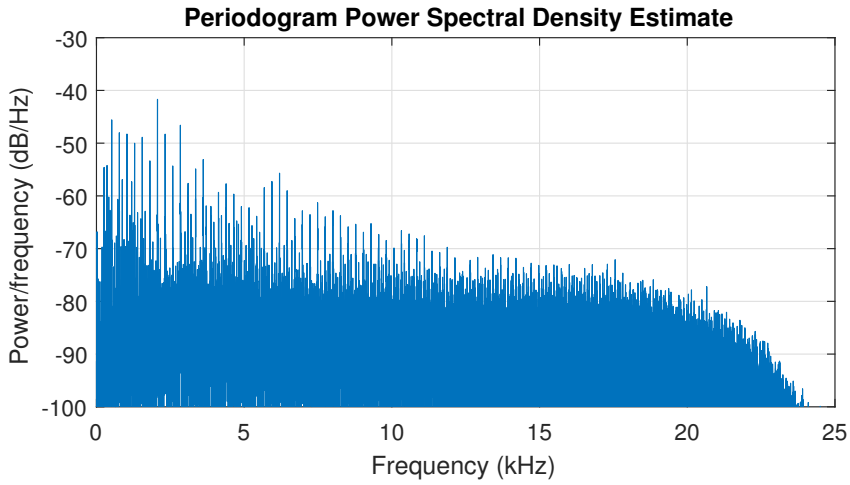


**Figure B.6:** Periodogram of 250Hz recorded tone, duty cycle 10.

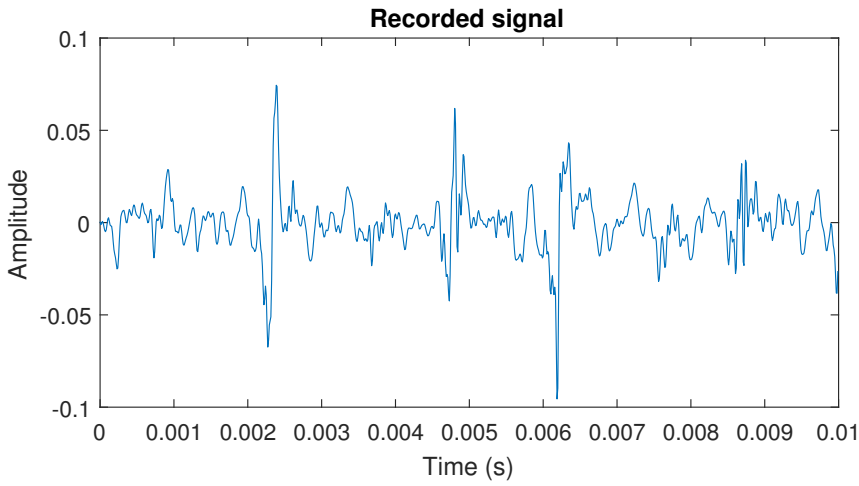


**Figure B.7:** Time domain plot of 250Hz recorded tone, duty cycle 09.

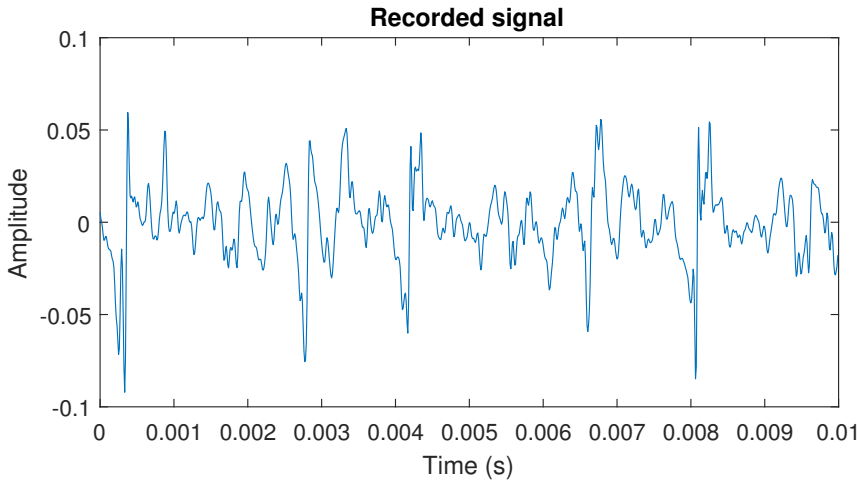


**Figure B.8:** Time domain plot of 250Hz recorded tone, duty cycle 10.

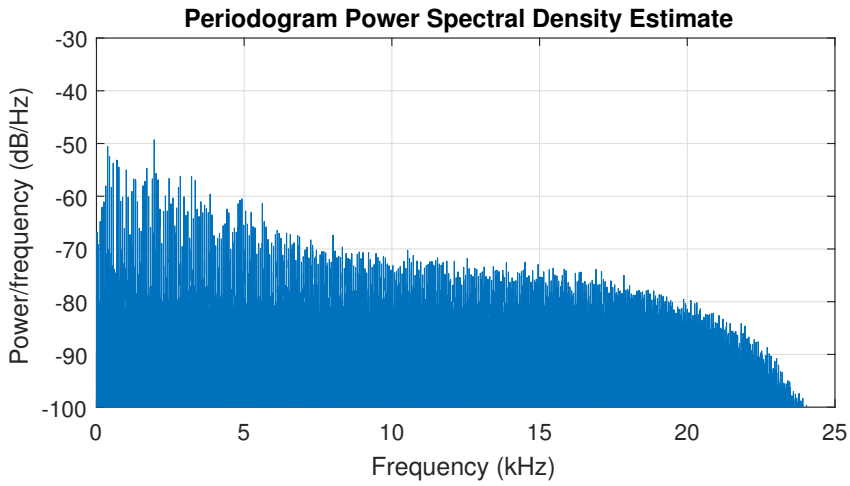


**Figure B.9:** Periodogram of 63Hz recorded tone, duty cycle 09.

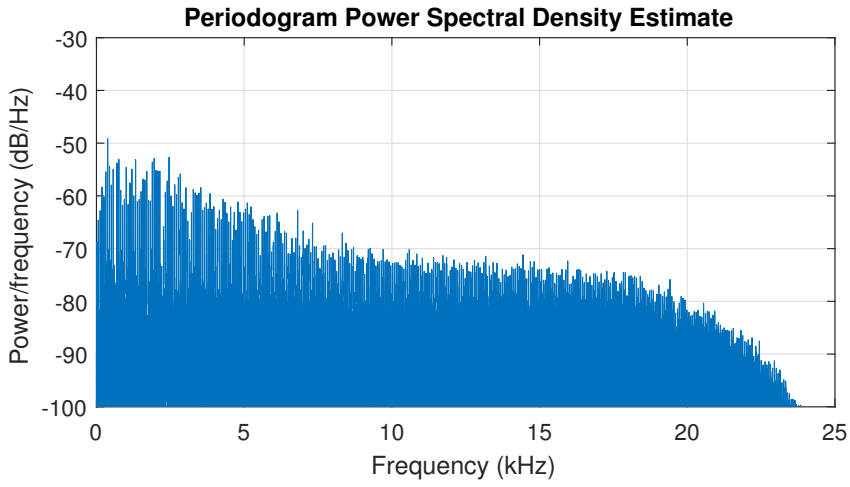


**Figure B.10:** Periodogram of 63Hz recorded tone, duty cycle 10.

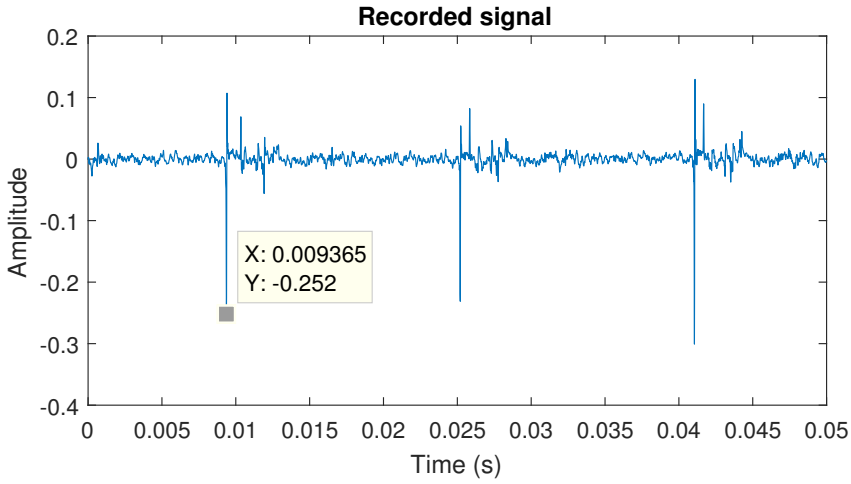


**Figure B.11:** Time domain plot of 63Hz recorded tone, duty cycle 09.

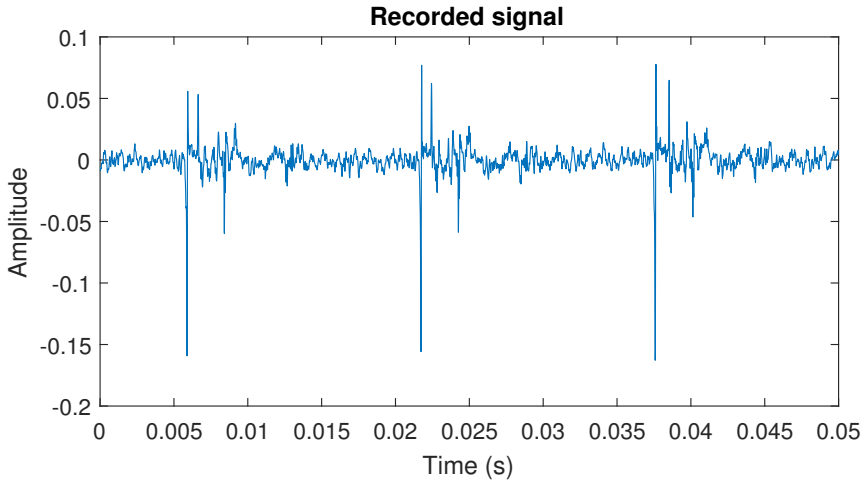


**Figure B.12:** Time domain plot of 63Hz recorded tone, duty cycle 10.